JOURNAL OF GEOPHYSICAL RESEARCH, VOL. 104, NO. E1, PAGES 1897–1916, JANUARY 25, 1999

Surface processes in the Venus highlands: Results from analysis of Magellan and Arecibo data

Bruce A. Campbell

Center for Earth and Planetary Studies, Smithsonian Institution, Washington, D.C.

Donald B. Campbell

National Astronomy and Ionosphere Center, Cornell University, Ithaca, New York

Christopher H. DeVries

Department of Physics and Astronomy, University of Massachusetts, Amherst

Abstract. The highlands of Venus are characterized by an altitude-dependent change in radar backscatter and microwave emissivity, likely produced by surface-atmosphere weathering reactions. We analyzed Magellan and Arecibo data for these regions to study the roughness of the surface, lower radar-backscatter areas at the highest elevations, and possible causes for areas of anomalous behavior in Maxwell Montes. Arecibo data show that circular and linear radar polarization ratios rise with decreasing emissivity and increasing Fresnel reflectivity, supporting the hypothesis that surface scattering dominates the return from the highlands. The maximum values of these polarization ratios are consistent with a significant component of multiple-bounce scattering. We calibrated the Arecibo backscatter values using areas of overlap with Magellan coverage, and found that the echo at high incidence angles (up to 70°) from the highlands is lower than expected for a predominantly diffuse scattering regime. This behavior may be due to geometric effects in multiple scattering from surface rocks, but further modeling is required. Areas of lower radar backscatter above an upper critical elevation are found to be generally consistent across the equatorial highlands, with the shift in microwave properties occurring over as little as 500 m of elevation. These surfaces are not simply characterized, however, by the absence of a highly reflective component. Surface morphology and radar-scattering properties suggest that a mantling deposit forms at the highest elevations, most likely by in situ erosion of the original rock. In Ovda Regio, this process mantles or has removed surface festoon structure at the 1- to10-m scale, implying a significant depth for the weathered layer. Similar radar-dark areas occur in Maxwell Montes but are apparently unrelated to the current topography of the region. Possible reasons for these observations include mass wasting from areas of steep slopes, compositional or age differences within the montes, vertical tectonic shifts of relict contacts, local topographic effects on surface temperature, or errors in the Magellan topography data in the rugged terrain. While there is evidence for some of these effects in the existing data, no single model at present appears to satisfy all occurrences of high-altitude, radar-dark terrain. New measurements of the surface and lower atmosphere chemistry of Venus are needed to further refine these conclusions.

1. Introduction

The highlands of Venus comprise only about one sixth of the planet's surface, but they differ dramatically in morphology from the more widespread plains. These upland areas can be loosely grouped into volcanic edifices, highly deformed crustal plateaus (tessera), and belts of parallel or subparallel ridges, valleys, and grabens [*Head et al.*, 1992; *Solomon et al.*, 1992]. The nature of the surface within the highlands inferred from microwave measurements is also markedly different from that in the lowlands, with most areas above a certain elevation having high radar backscatter. The presence of these radar-bright features on Venus was recognized in the earliest Earth-based radar imaging and led to the naming of Alpha, Beta, and Maxwell. More detailed altimetry and mapping by the Pioneer-Venus Orbiter, Venera 15/16, and the Arecibo radar system illustrated the range of structures that comprise the highlands, and the global coverage and high resolution of the Magellan data have permitted more detailed mapping and analysis of surface properties [cf. *Campbell et al.*, 1983; *McGill et al.*, 1983; *Barsukov et al.*, 1986; *Saunders et al.*, 1992].

One of the most intriguing results of the Pioneer-Venus mission came from thermal emission maps and near-nadir radar echoes measured by the orbiter. These maps indicated

Paper number 1998JE900022.
0148-0227/99/1998JE900022$09.00

that virtually all areas on Venus above ~6054 km in planetary radius exhibit low microwave emissivity and high Fresnel reflectivity [*Pettengill et al.*, 1988]. These results were supported by Earth-based observations and confirmed by the Magellan mission [*Campbell et al.*, 1983; *Jurgens et al.*, 1988; *Pettengill et al.*, 1992]. The much finer spatial resolution of the Magellan altimeter and radiometer make it possible to study local changes in these properties with elevation and surface geology. Analysis of the altitude-emissivity trends for plateaus and volcanoes showed that the change in surface properties occurs rapidly with elevation above a lower critical radius (which we term H_L), which was inferred to vary with the maximum height of a given region [*Klose et al.*, 1992]. Stereo-derived topographic data for Ovda Regio were used by *Arvidson et al.* [1994] to infer the presence of a second upper critical altitude, referred to here as H_U, at ~6056 km, above which surface properties return, over perhaps a 500-m elevation range, to more normal (plains-like: Fresnel reflectivity ~0.10, horizontal-polarized emissivity ~0.84) values.

Theoretical considerations of possible candidate materials and processes that might explain these observations have been numerous, with suggestions of pyrite, ferroelectric minerals such as perovskite, and cold-trapped halides or chalcogenides [*Shepard et al.*, 1994; *Brackett et al.*, 1995; *Fegley et al.*, 1992, 1997; *Wood*, 1997]. Recent bistatic radar measurements and theoretical analyses suggest a single dielectric interface, rather than volume scattering, but no consensus on a candidate mineral or coating has yet emerged [*Pettengill et al.*, 1996; *Tryka and Muhleman*, 1992; *Wilt*, 1992]. These modification processes have varying timescales over which they may act on the surface, from very rapid for the temperature-dependent dielectric changes of ferroelectric minerals [*Shepard et al.*, 1994] to relatively slow for the vapor-phase deposition model [*Brackett et al.*, 1995]. On the basis of studies of surfaces near H_L and the absence of parabolic ejecta deposits in the highlands, *Arvidson et al.* [1992] estimated that formation of highly reflective material proceeds at less than 10^{-2} μm/yr.

Different geologic interpretations have been made for areas that do not follow the average altitude-emissivity trend. For example, the absence of a strong dielectric change for Maat Mons has been interpreted to imply a relatively young age for the upper surface of this volcano [*Klose et al.*, 1992; *Robinson and Wood*, 1993; *Robinson*, 1995]. *Basilevsky and Head* [1995] suggested that low radar-return areas in Maxwell Montes are evidence for differing rock composition. It is important to note, however, that both the temporal and spatial variability of highly reflective material formation are unknown; there may have been changes in the rate of formation (or complete cessation of this process) during the history of the observable surface.

In this paper, we analyze Magellan radar images and estimates of emissivity and Fresnel reflectivity for major Venus highland regions. These data are augmented by high-resolution Arecibo images collected in 1988, which offer complementary incidence angles and both linear and circular polarization modes. These data sets are used to characterize the range of scattering/emission behavior within the highlands, their broad correlation with topography, and possible implications for surface properties. We then study the local morphology of areas above the upper critical elevation and propose a model for the development of a surface mantling layer. Finally, we examine regions whose properties differ from the global average and assess possible mechanisms for these variations.

2. Microwave Data Sets

The Magellan spacecraft utilized its primary radar antenna to collect both 12.6-cm-wavelength synthetic aperture radar (SAR) images and measurements of the passive thermal emission from the surface. Radar image coverage of most of the planet was accomplished in the nominal left-looking SAR incidence angle profile and HH polarization, but during later cycles a variety of more limited observations were made in the VV polarization and using incidence angle profiles that permit stereo viewing [*Saunders et al.*, 1992]. Emission observations were converted to estimates of emissivity by reference to an assumed standard lapse rate for the Venus atmosphere [*Pettengill et al.*, 1992]. The smaller altimeter horn antenna was used to collect near-nadir observations of radar backscatter, which were modeled by *Ford and Pettengill* [1992] using *Hagfors'* [1964] expression for echoes from gently undulating surfaces to obtain estimates of planetary radius H, Fresnel reflectivity ρ_0, and root-mean-square (rms) slope θ_{rms}. The slope distribution and near-nadir backscattering behavior of the surface were also modeled by *Tyler et al.* [1992] using a different inversion method.

The Fresnel reflectivity and surface emissivity can both be related to the dielectric constant ε of the surface, but such estimates are intrinsically model dependent. The surface emissivity E is related, to a degree that varies with the viewing geometry, to the dielectric constant and wavelength-scale roughness [*Pettengill et al.*, 1992; *Campbell*, 1994]. The Fresnel reflectivity can be converted to a value for ε, but the derivation of ρ_0 must include a correction for the estimated effects of diffuse surface scattering. The Magellan emissivity data have a spatial resolution of 20-30 km in the equatorial region, while the altimeter footprints for the same area are typically ~10 km. We check results from both data sets throughout this work.

The Earth-based radar data used here were collected in 1988 at Arecibo Observatory. A single mode of circular polarization was transmitted, and both senses of polarization were received. Delay-Doppler mapping of multiple observations at 8 μs pulse length provided nine looks at 2.1 km/pixel resolution for the northern hemisphere and 20 looks at the same resolution for the southern hemisphere. For each look, the value of measured backscatter in a region of empty space was used to estimate the noise level within the scene, and each look was corrected by its respective background level prior to averaging. This provided a greatly improved estimate of the ratio between "polarized" (LR or RL) and "depolarized" (LL or RR) echoes, even in areas of relatively low backscatter strength. The letter pair designations refer to the transmitted and received polarization states (L and R for left and right circular, H and V for horizontal and vertical plane polarization). A series of calibration steps (Appendix 1) was then implemented to convert the data to units of backscatter cross section per unit area σ^o. Separate, linearly polarized data (analogous to HH and HV values) were also collected for the area surrounding Maxwell Montes, but we did not attempt any absolute calibration of these data. For all work presented here, the Arecibo data have been further averaged to 8 km resolution

(144 looks in the northern hemisphere) to reduce the effects of noise on the polarization ratios.

A primary issue in highlands analysis is the true planetary radius of specific sites. The Magellan Global Topographic Data Record (GTDR) was created by resampling the raw altimetric data to a 5.4-km spatial resolution, but this produced a few highland areas with apparently anomalous local changes in elevation. We examined the individual Magellan altimeter echo traces surrounding these points and found that some abrupt changes in height stem from the inclusion of footprints with multiple peaks or very low peak-to-background signal ratios. The problem is most acute in areas of mountainous topography (which present a problem for any radar altimeter) and in regions with mixtures of low-radar-return and high-return terrain. In these cases, the off-nadir echoes may be just as strong as the desired subspacecraft signal, and the altimeter template-fitting algorithm may select a spurious peak [*Ford and Pettengill*, 1992]. We developed a first-order parameter, similar to the Massachusetts Institute of Technology (MIT) footprint signal-quality indicator (SQI), for the reliability of any given Hagfors model template fit (Appendix 2) and used it to exclude those footprints with very poor behavior. The remaining database was then smoothed with a Gaussian weighting filter 0.15° (~16 km) in radius. This reduced the spatial resolution of the final maps relative to the GTDR but removed most of the spurious values. These smoothed data were used only in the production of profiles across the highlands; the global correlations discussed herein were made using the GTDR maps.

3. Backscatter and Polarization Properties

In this section, we review the global average correlation of altitude and microwave properties on Venus and add to these results data for the linear and circular radar polarization ratios at 12.6 cm wavelength. We then compare backscatter curves for the highlands to those of terrestrial volcanic terrain as an indicator of the surface-scattering regime.

3.1. Global Properties

Any discussion of the altitude dependence of microwave behavior must take into account the nonuniform distribution of elevation with latitude. There is a gap between about 45° and 65° latitude in both hemispheres for which little terrain exceeds a radius of 6054 km, and the southern hemisphere high latitudes also contain almost no areas above this radius. Because of this spatial bias, our only view of highland surfaces at high latitudes is provided by Ishtar Terra. Likewise, instances of topography above ~6056-km radius in the equatorial region are limited primarily to Theia, Rhea, Tepev, Ozza, Sapas, and Maat Montes and portions of Ovda Regio. Radius values above ~6058 km in the equatorial belt are found only on Maat Mons.

The average 12.6-cm emissivity and model-derived Fresnel reflectivity for Ishtar Terra and the equatorial region (±40° latitude) of Venus are shown in Figure 1. For the equatorial region, the average emissivity and reflectivity indicate an increasing dielectric constant (increasing ρ_0, decreasing E_h) above H_L~6054 km and a rapid shift back to more plains-like values near 6056 km [*Arvidson et al.*, 1994]. For Ishtar Terra, the lower critical elevation shifts upward to ~6056 km. The

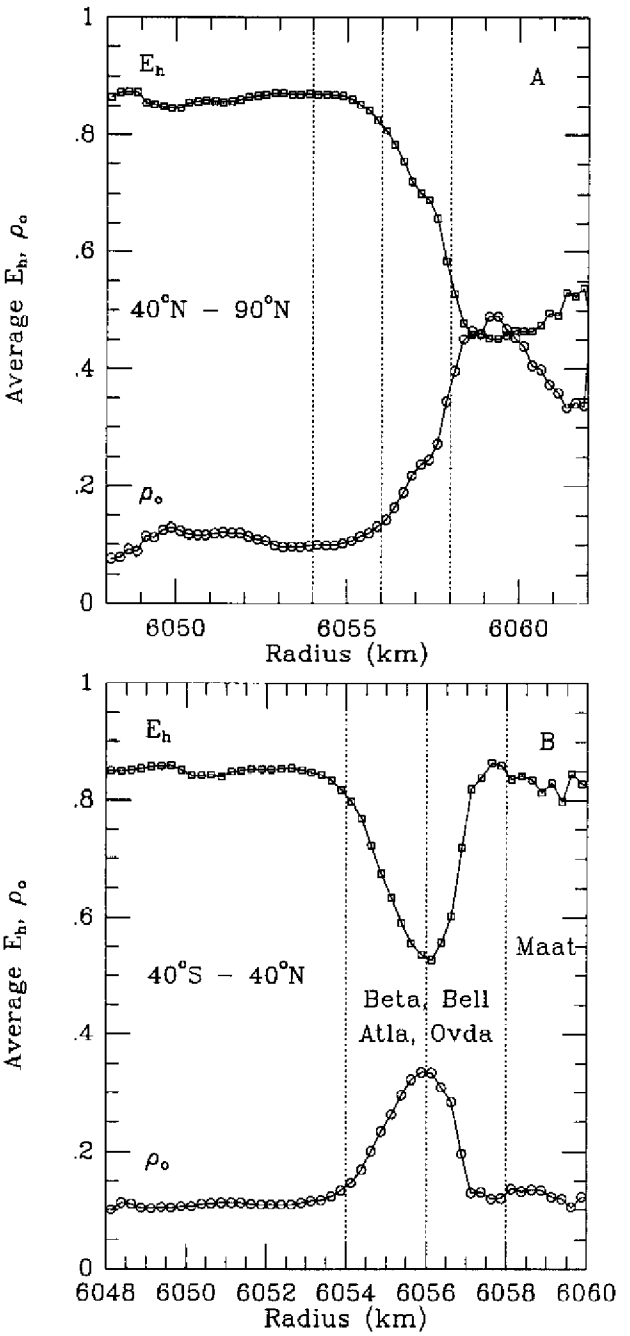

Figure 1. Average horizontal-polarized emissivity E_h and corrected Fresnel reflectivity ρ_o as a function of elevation for two latitude ranges on Venus. Topography is divided into 250-m bins. (a) Northern latitudes (Ishtar Terra), >40°N. (b) Equatorial regions, 40°S - 40°N.

average emissivity reaches a minimum at ~6059 km, then increases slightly for values of H>6060 km. Likewise, the average ρ_0 values decrease to about 0.35 in the highest parts of Maxwell Montes after peaking near 6059 km. There is thus no clear upper critical elevation within Maxwell Montes analogous to that observed in the equatorial region. The systematic 2-km shift in H_L from the equator to Ishtar Terra has been suggested by *Pettengill et al.* [1996] as an indicator of higher temperatures toward the poles, but the biased spatial distribution of venusian highlands prevents a rigorous test of this possibility.

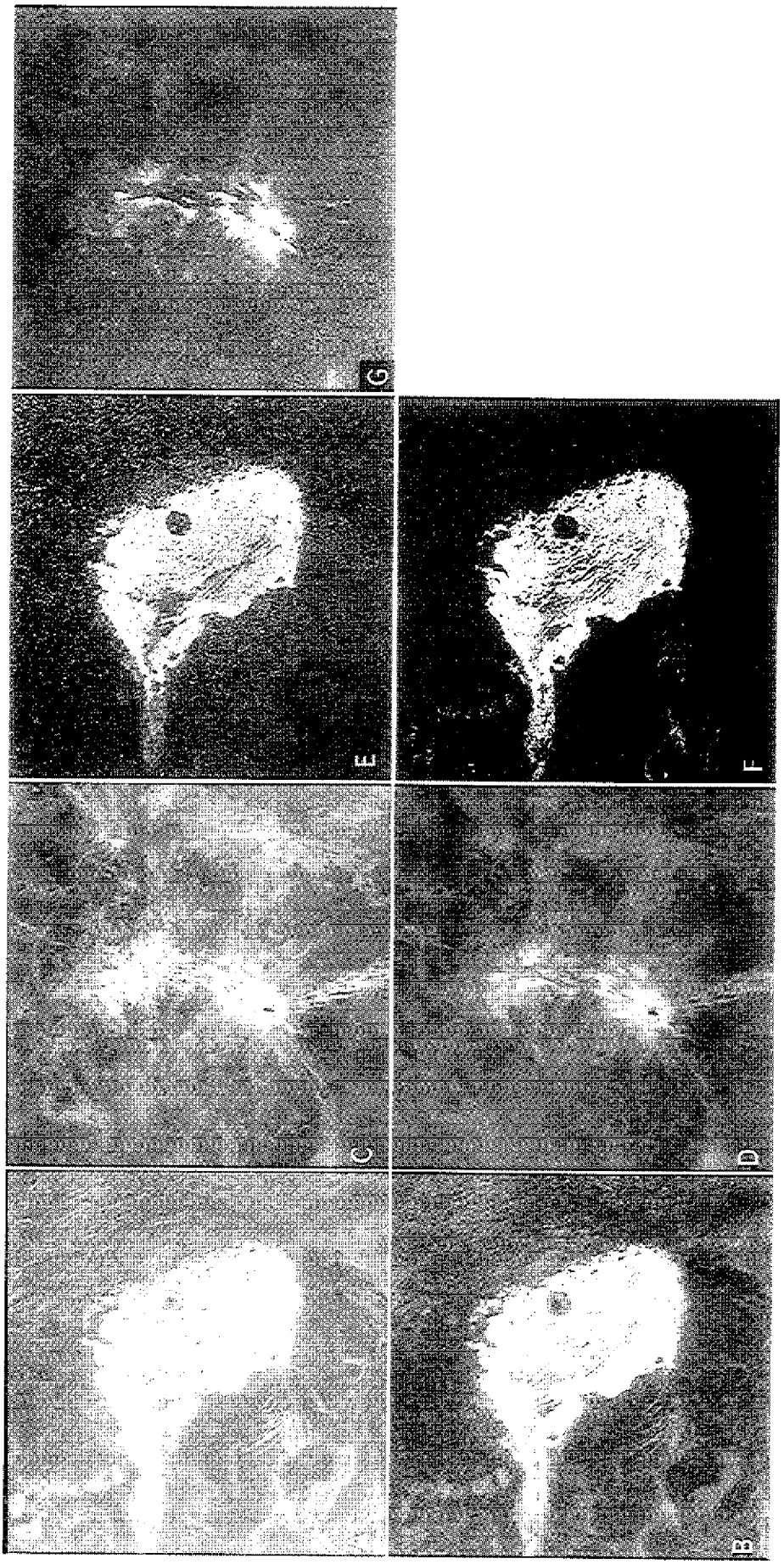

Figure 2. Arecibo dual-polarization radar images of Maxwell Montes and Beta Regio. (a) Maxwell polarized (LR) data. (b) Maxwell depolarized (LL) data. (c) Beta polarized (LR) data. (d) Beta depolarized (LL) data. (e) Maxwell circular polarization ratio μ_C (LL/LR). (f) Maxwell linear polarization ratio μ_l. These values have been clipped to zero for areas with low depolarized cross section (i.e., Lakshmi Planum and the dark areas in northwestern Maxwell). (g) Beta circular polarization ratio μ_c.

3.2. Polarization Ratios

The Arecibo Observatory data can be used to derive values for the circular polarization ratio μ_C (the ratio of depolarized circular power to the polarized sense, LL/LR). For the region surrounding Maxwell Montes, separate observations were made using orthogonal senses of linear polarization. The linear polarization ratio μ_l calculated from these measurements is analogous to the HV/HH parameter, but we do not know the actual polarization angle between the incident beam and the surface (e.g., whether the incoming radar beam is H or V polarized). For most rough rocky surfaces, however, the HV/HH and VH/VV ratios are relatively similar [*Campbell et al.*, 1993]. Polarization ratios are often used in radar studies to analyze the degree of diffuse or multiple scattering from a target surface [cf. *Ostro et al*, 1992; *Campbell et al.*, 1993].

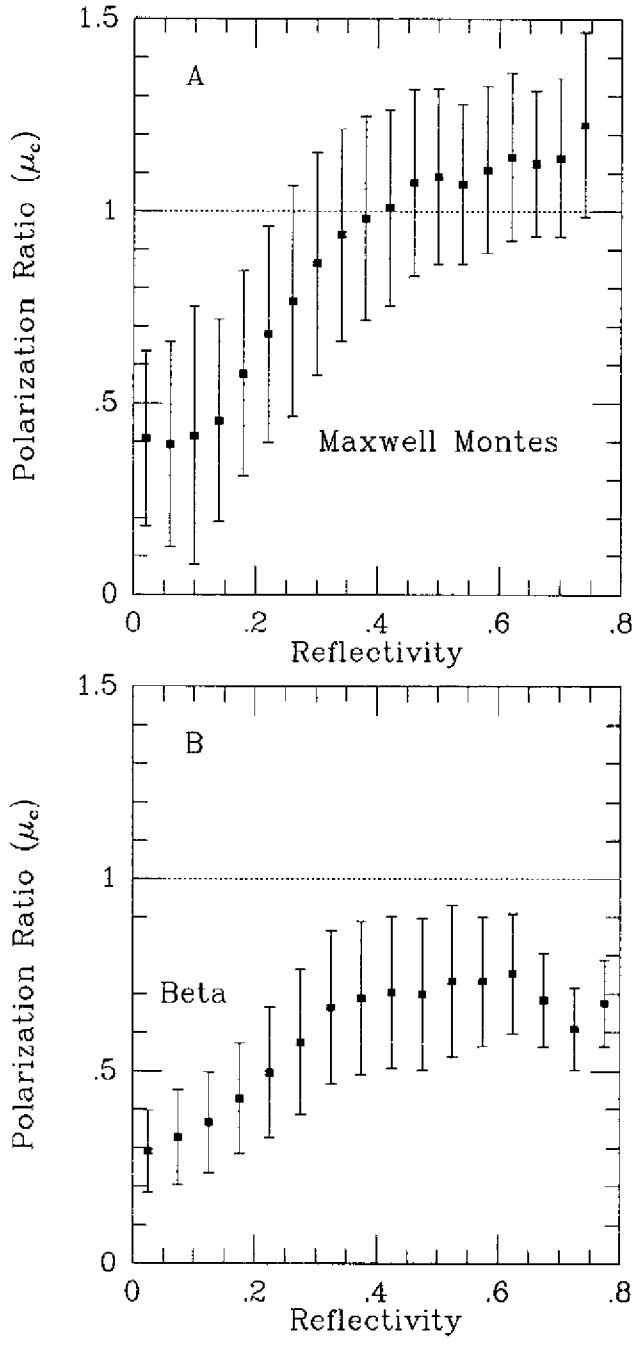

Figure 3. Average circular polarization ratio as a function of reflectivity for (a) Maxwell Montes and (b) Beta Regio. Note that μ_C values greater than unity are common in very highly reflective areas of Maxwell. Error bars indicate 1 standard deviation.

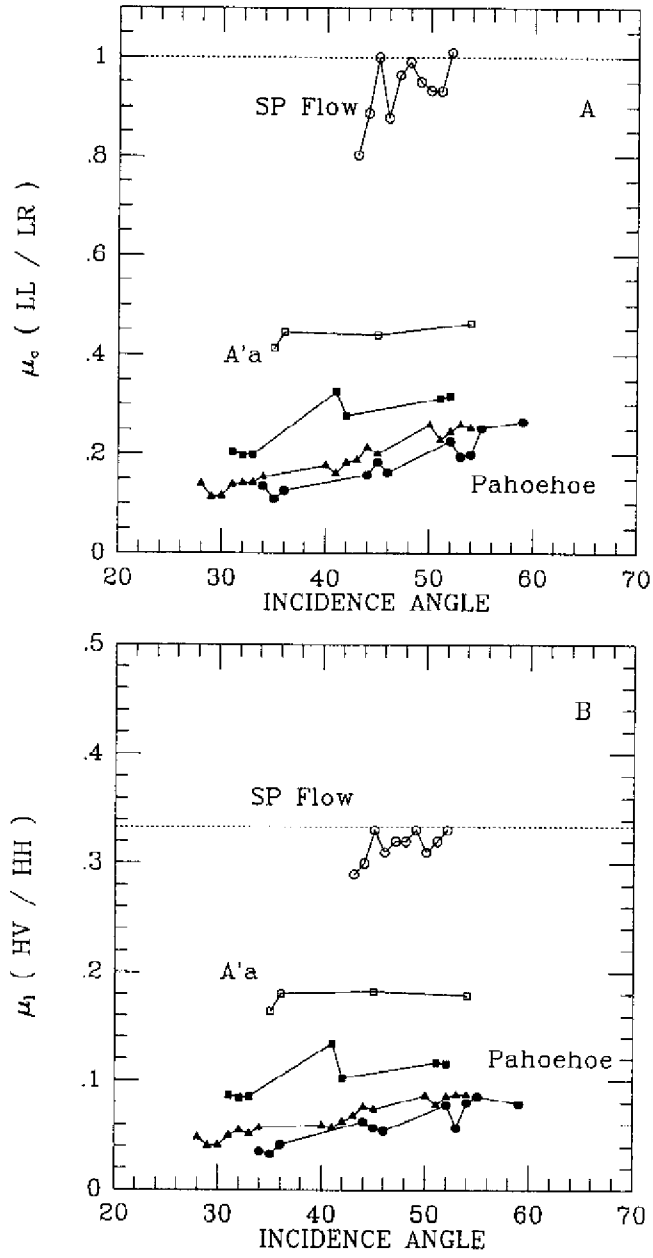

Figure 4. Polarization ratios for terrestrial surfaces. Data are for synthesized 12.6-cm wavelength measurements [*Campbell and Campbell*, 1992], with the exception of the SP flow observations (24-cm wavelength). A'a surfaces are rough, with up to 10 cm rms height at the 1-m scale; pahoehoe flows are smooth, with rms heights as low as 0.5 cm at the 1-m scale. (a) Circular polarization ratio μ_C. Note the limiting value of ~1. (b) Linear polarization ratio μ_l. Note the limiting value of ~1/3.

Beta Regio and Maxwell Montes are the largest highly reflective areas covered by the Arecibo data, and polarization ratio images for these two areas are shown in Figure 2. We also calculated average values of μ_C as a function of model-

derived Fresnel reflectivity for the two sites (Figure 3). Values of μ_c increase with ρ_o and exceed unity in many areas of Maxwell Montes, reaching a maximum of 1.3. Average values of μ_c for Beta Regio also increase with reflectivity but only reach a maximum of about 0.75. The linear polarization ratio for Maxwell increases with reflectivity, reaching a maximum value of about 0.5. *Haldemann et al.* [1997] found 3.5-cm-wavelength circular polarization ratios of 0.5-0.8 for Beta Regio, consistent with the Arecibo 12.6-cm values.

Polarization ratios for terrestrial lava flows (Figure 4) provide a comparison to the Arecibo data [*Campbell and Campbell*, 1992]. In general, rougher surfaces have higher μ_c and μ_l values, and these ratios increase slowly with incidence angle. The difference in μ_c between Beta Regio and Maxwell Montes is thus likely due to the smaller Arecibo incidence angle (ϕ=50-55°) for Beta relative to that for Maxwell (up to 75°). Values of μ_c=1 and μ_l=1/3 are typically upper limits on the average ratios for extremely rough surfaces or those imaged at very high incidence angles, and these values are consistent with diffusely scattered echoes, represented by a model of randomly oriented, small dipole elements. Local regions of very blocky lava flows, such as SP in Arizona, have circular polarization ratios of up to 2, likely owing to double reflections from dihedral joints created by the smooth-sided blocks [*Campbell et al.*, 1993]. Values of μ_c greater than unity are also observed for ices, where subsurface multiple scattering is presumed to be a significant component of the radar return [*Ostro et al.*, 1992; *Rignot*, 1995].

Previous observations of the highlands circular polarization ratio by *Tryka and Muhleman* [1992] were interpreted as evidence for coherent volume scattering within a low-loss matrix [e.g., *Hapke*, 1990]. The coherent backscatter mechanism may produce a decline in μ_l as the HH echo is preferentially enhanced relative to the HV return, but the opposite effect is observed at Maxwell. Additional concerns regarding the need for potentially unrealistic radar-transparent matrix material in the coherent scattering scenario were raised by *Wilt* [1992]. Surface multiple scattering could instead produce the observed polarization properties, with the increased dielectric constant leading to more efficient second-, third-, and higher-order reflections. Double-bounce echoes between rock faces produce significant depolarization of an incident wave, and the extreme case of this is dihedral structures such as those observed at SP flow [*Hagfors and Campbell*, 1974; *Campbell et al.*, 1993]. We suggest that the high circular and linear polarization ratios on Venus are due to an increasingly strong surface multiple-scattering component related to the increased reflectivity. This hypothesis is consistent with the bistatic radar data analyzed by *Pettengill et al.* [1996], which imply a predominantly surface-scattering mechanism for portions of Maxwell.

3.3. Angular Backscatter Functions

The shape of the angular radar scattering function is dependent in part on surface roughness, and the combination of Magellan and Arecibo data cover a wide range of incidence angles. Magellan cycle 1 and cycle 3 data provide values of σ^o at incidence angles of about 25° and 32° for Maxwell Montes, while Arecibo views this area at ~70°. Backscatter cross sections averaged over 11 rectangular sample areas are shown in Figures 5a and 5b. Also plotted is the Venus-average Muhleman scattering curve and estimates of the S band HH

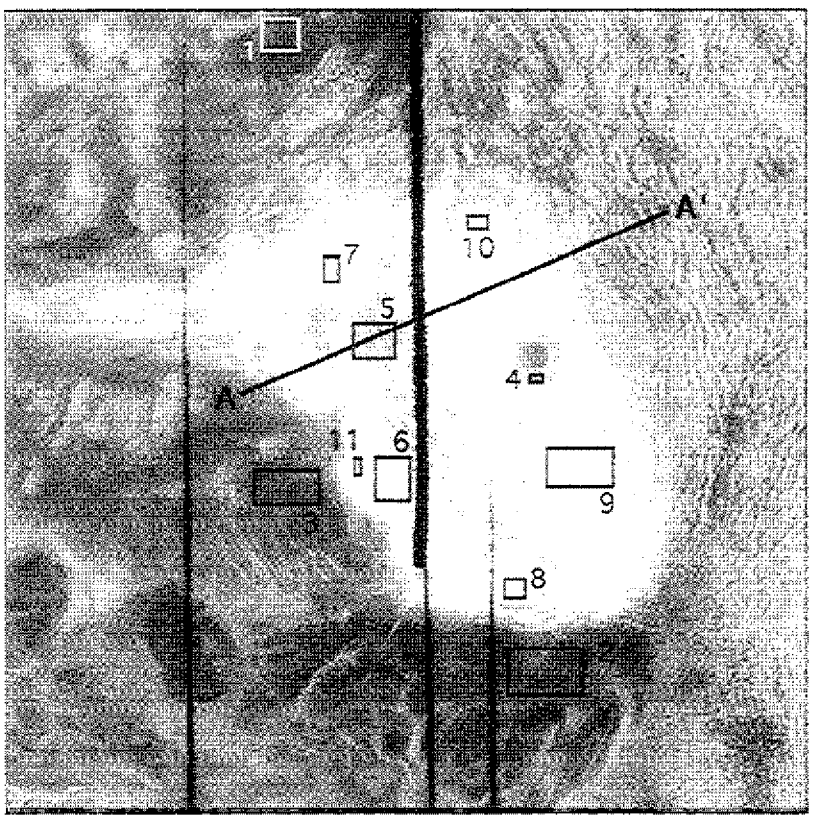

Figure 5a. Map of sample site locations for Maxwell Montes. Profile A-A' corresponds to data in Figure 18. North is at the top.

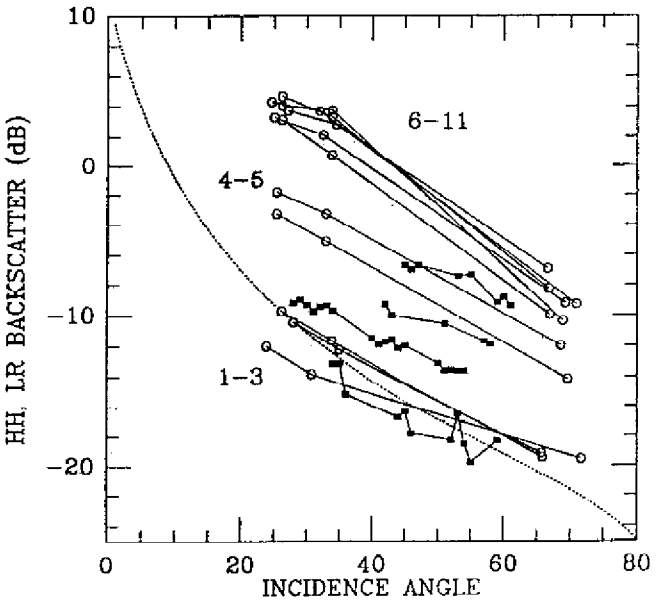

Figure 5b. Scattering coefficient as a function of incidence angle for 11 sites in Maxwell Montes. Note the behavior of the bright highland surfaces, which have a significant drop in power between 30° and 70°. Solid symbols denote data for four Hawaiian lava flows [*Campbell and Campbell*, 1992] from a smooth low-return pahoehoe (1 cm rms height at 1-m horizontal scale) to a rugged radar-bright a'a surface (8-cm rms height at 1-m scale).

echo for four Hawaiian lava flows with rms heights, at the 1-m horizontal scale, of 1-8 cm [*Campbell and Shepard*, 1996].

The brighter areas in Maxwell have radar cross sections well above those of the rough lava surfaces, consistent with much of the increased echo being due to enhanced Fresnel reflectivity. More anomalous is the large decline in σ° for these areas between ~30° and 70° incidence angle. Angular backscattering functions for Beta Regio show the same behavior. It is interesting to note that a rough or strongly multiple scattering surface, which we predicted based on the circular and linear polarization ratios, is expected to have little variability in σ° with incidence angle. No simple explanation can be offered for these scattering properties, and further theoretical analysis of possible multiple-scattering situations or unmodeled systematic errors in the Arecibo data at high angles is required.

4. Surfaces Above the Upper Critical Radius

As noted by *Arvidson et al.* [1994], there exists at Ovda Regio a transition in microwave properties from high reflectivity back to more plains-like properties near 6056-km radius, which they attribute to the temperature-dependent behavior of a ferroelectric material. We first examine other highland regions along the equatorial belt to determine whether this behavior is consistent in altitude, then consider the surface morphology and radar properties of these radar-dark features as a guide to their possible formation mechanism.

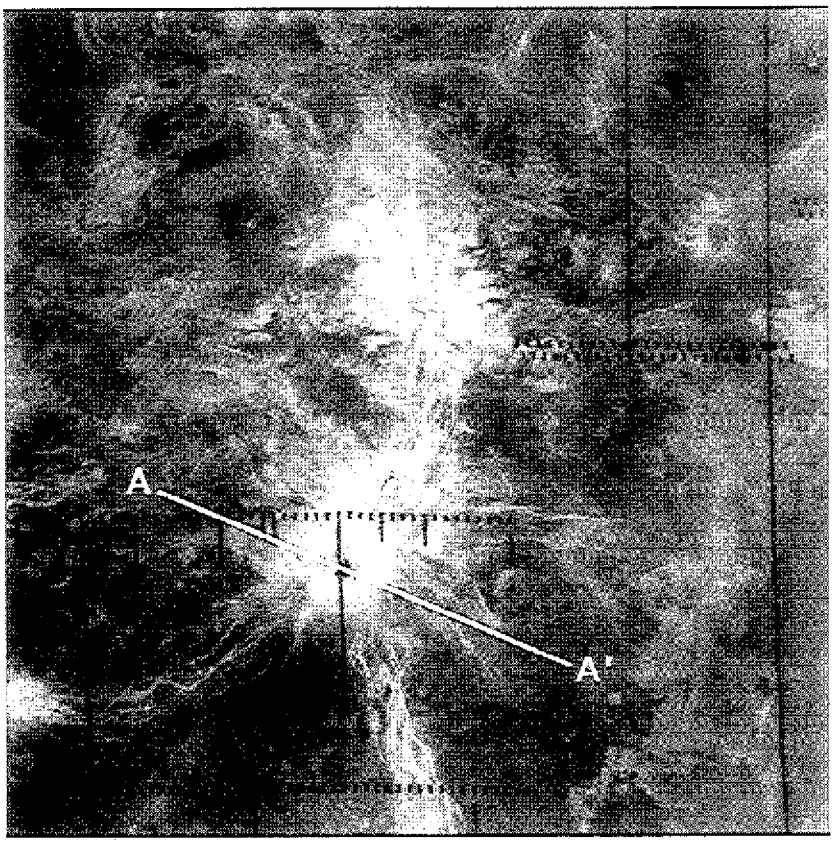

Figure 6a. Magellan radar image of Beta Regio (14-41°N, 268-298°E). Location of profile corresponds to data in Figure 6b. Arrows denote regions of high-altitude, low backscatter behavior. North is at the top.

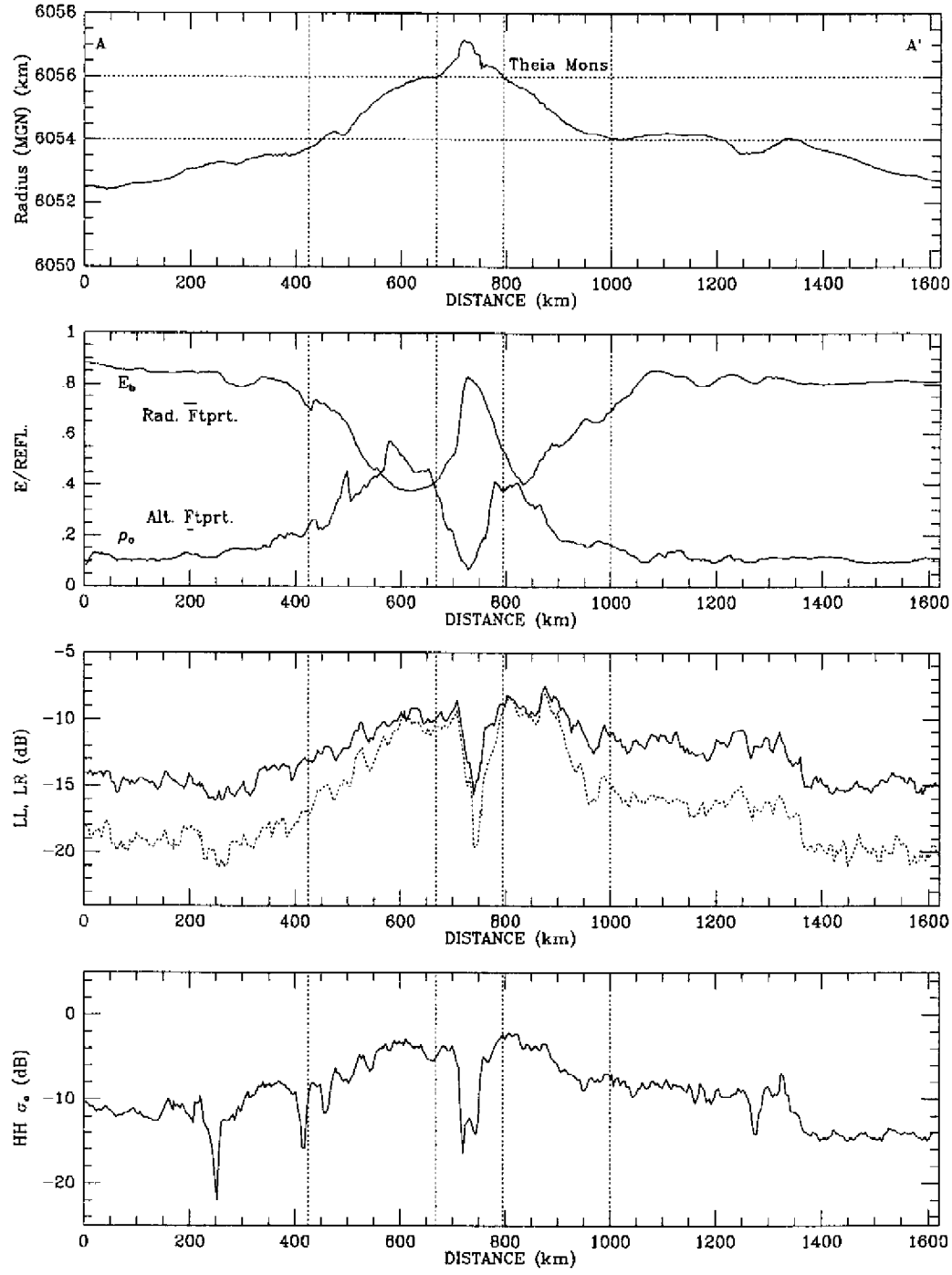

Figure 6b. Profile (averaged over a 40 km wide swath) of remote sensing data for Theia Mons (A-A' in Figure 6a). Note the lower critical elevation of 6054 km and the drop in radar brightness and reflectivity at the summit (H>6056 km). Data are plotted for planetary radius, emissivity, Fresnel reflectivity, LL (dotted) and LR (solid) backscatter cross section, and HH backscatter cross section. The approximate size of the Magellan altimeter and radiometer footprints at this latitude are shown by the scale bars.

The three major equatorial uplands with low radar-return summit areas are Beta, Ovda, and Atla Regiones. With the exception of Maat Mons, we found very consistent properties near the postulated upper critical radius in all three regions. The upper transition altitude is between 6056 and 6057 km at Theia Mons and along the margins of Devana Chasma (Figures 6a and 6b), across Ovda Regio as shown by *Arvidson et al.* [1994], and at the summit of Ozza Mons and along the margins of Ganis Chasma (Figures 7a and 7b). This suggests that the change in properties is linked to the stability of a particular mineral assemblage as a function of temperature and pressure and that the composition of the equatorial highlands is either consistent across the three study areas or has little impact on the formation of the highly reflective component. The surface morphology and scattering properties of areas above the upper critical radius is also similar, as shown by several examples.

The highest-standing areas of Ovda Regio, shown in Figure

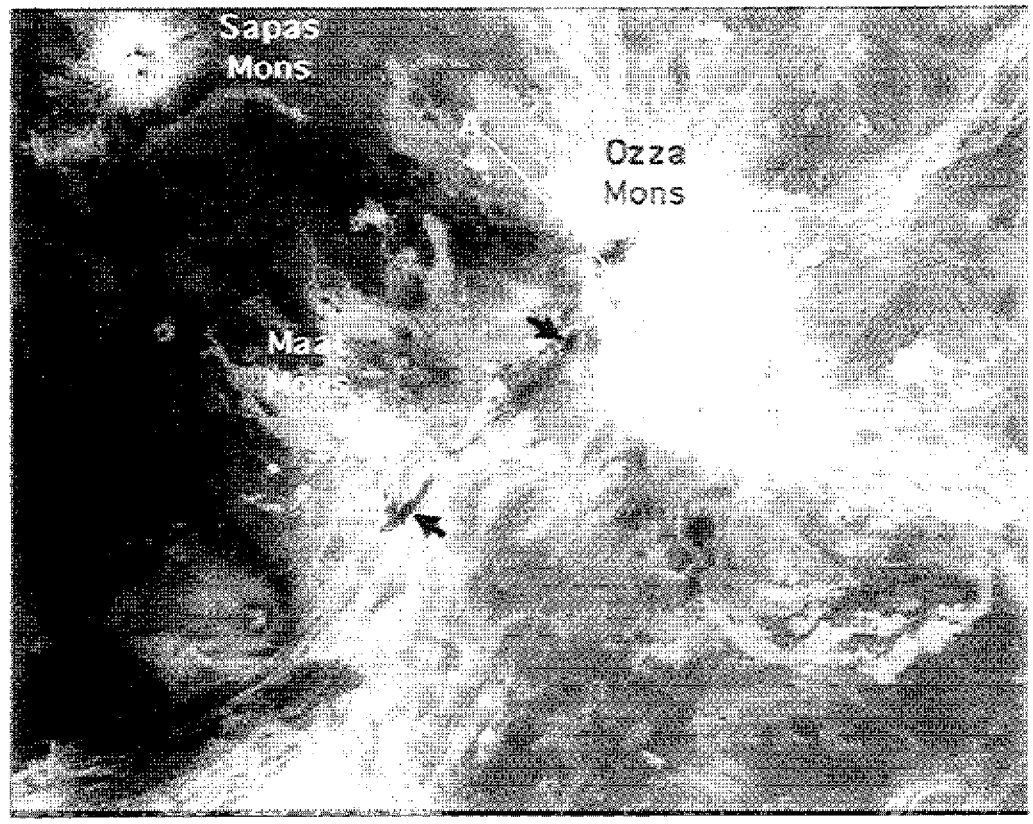

Figure 7a. Magellan radar image of Atla Regio (185°-210°E, 10°S-10°N) with profile shown in Figure 7b marked. Arrows denote radar-dark patches at high elevations. North is at the top.

8a, are a combination of tessera terrain and very thick lava flows that superpose the tessera and were in turn affected by later tectonic deformation [*Pettengill et al.*, 1992]. There are three major units in this region: (1) tessera, characterized by varying degrees of compressional and/or extensional tectonic deformation; (2) a "festoon" lava flow with thick lobate margins and high radar backscatter (similar to a deposit studied by *Moore et al.* [1992]); and (3) a thick lobate flow with low radar return (Figure 8b). These latter two units are likely part of the same flow complex, with the differences in surface properties due to changes in elevation. Unit 2 superposes the older tessera structure, is of the order of 50 to a few hundred meters deep based on the bright radar reflections from its steep margins, and has large arcuate surface ridges that likely run perpendicular to the direction of local lava motion during emplacement. Unit 3 also has thick flow margins but little, if any surface structure at the hundreds of meters scale.

Arvidson et al. [1994] showed that the shift in radar brightness across the festoon flow follows a topographic contour rather than any obvious geologic contact, but there are some places where a thick flow margin fortuitously lies near H_0. The change from high to low backscatter, which we infer to correlate with a change in surface dielectric constant, occurs everywhere over only a few hundred to perhaps 500 m in elevation. This is best demonstrated in the western distal portions of unit 3 (Figure 9). Flow lobes in this area have been cut by grabens, and portions of the flow have been downdropped by perhaps a few hundred meters (same-side stereo data do not exist for this area). These shifts in elevation produce a large change in radar brightness, indicating that the dielectric constant of the surface is transitioning between the highly reflective state and the more normal condition.

Figure 10 shows detail of the northern boundary between radar-bright and higher-standing radar-dark deposits. In the middle of this image (within the bright area), there are distinct interior ridges, which indicate that the flow moved from southeast to northwest. It appears that the radar-bright and radar-dark flow materials are part of the same unit, since there is no sharp lobate contact between them. Where the surface elevation exceeds H_0, the lava flow texture changes dramatically. There is no evidence in the radar-dark portions of the flow for ridges or other structures, and even the large valleys that have formed owing to extensional tectonism appear subdued (note the southeast corner of Figure 10). The smooth texture of this flow is unexpected; thick lobate lava flows on Earth, usually associated with silicic volcanism, are characterized by rough morphology and large surface ridges.

This deposit may be an example of a unique volcanic morphology on Venus, characterized by very thick flow lobes and low surface roughness, but this model cannot explain the lack of a clear boundary between the radar-dark and radar-bright areas, nor the low radar return from tessera terrain south and east of the radar-dark flow. Were the surface compositionally different from the festoon flow to the north, we would expect to see the change in surface properties follow the outlines of the flow, whereas *Arvidson et al.* [1994] showed that elevation is the controlling factor in this change. The same argument holds for pyroclastic mantling deposits, which would not tend to follow a topographic contour. We instead suggest that the process that produces the high-reflectivity effect between 6054-

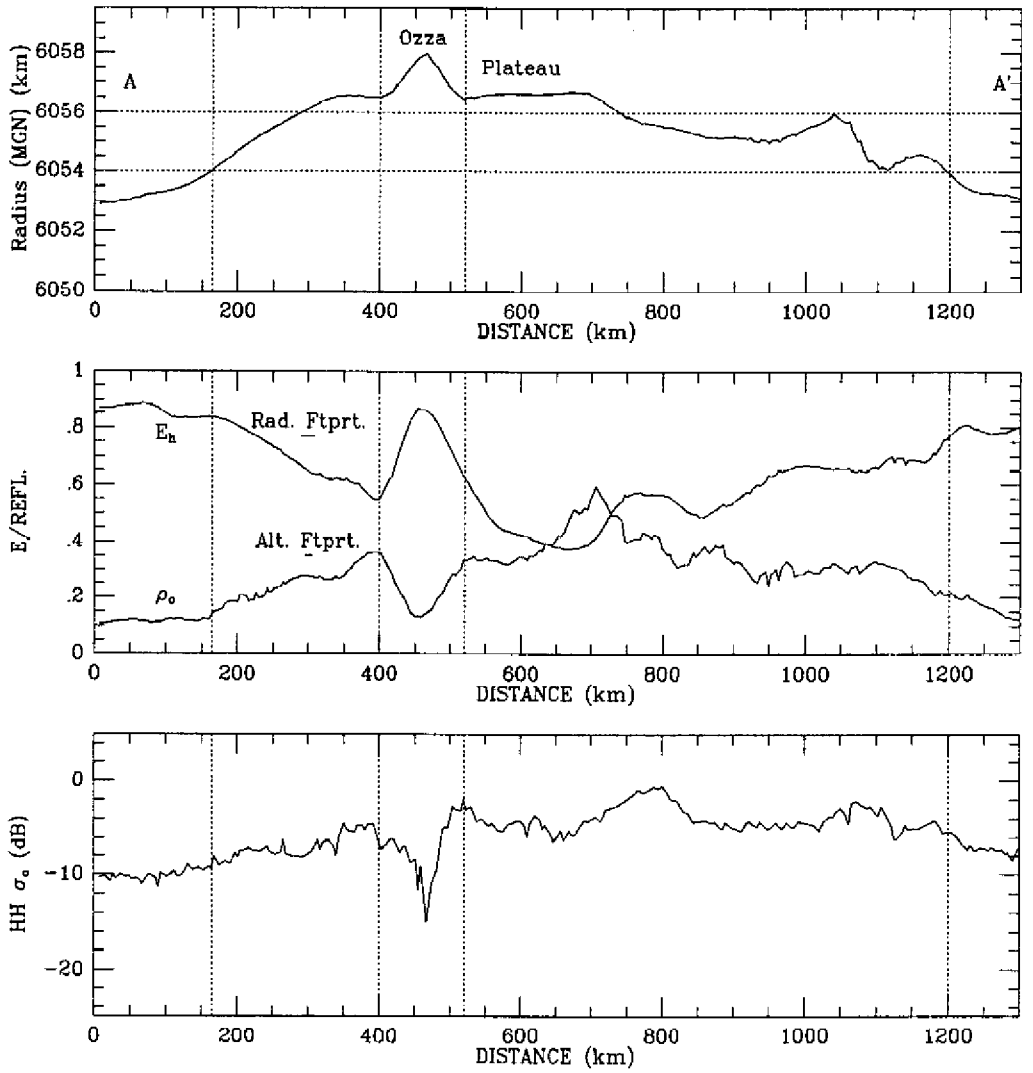

Figure 7b. Profile (averaged over a 40-km wide swath) of remote sensing data for Ozza Mons (A-A' in Figure 7a). Note the very low emissivity for the plateau just south of the summit, which lies at 6056- to 6057-km radius. Data are plotted for planetary radius, emissivity, Fresnel reflectivity, and HH backscatter cross section. The approximate size of the Magellan altimeter and radiometer footprints at this latitude are shown by the scale bars.

and 6056-km radius also leads to the development (either depositional or erosional) of porous mantling layers at elevations above H_U. This implies fine-grained deposits or locally derived sediments up to several meters thick to mantle or remove the preexisting topography. It is interesting to note that the festoon texture does not "reappear" in areas where the flow lobes have been downdropped (Figure 9), suggesting that the weathering process does, in fact, erode the original structure.

The summit region of Theia Mons (Figure 11), approximately 20 x 60 km in extent, is characterized by emissivity and Fresnel reflectivity values close to the planetary mean. The surface of the summit is composed of low-relief, presumably volcanic, material that is broken into large polygonal sections [e.g., *Campbell et al.*, 1984; *Stofan et al.*, 1989; *Senske et al.*, 1991; 1992]. To the north, south, and west, the dark material is bounded by steep scarps indicative of slope failure. On the eastern side, the dark materials appear to extend over the edifice flanks and were dissected by N-S trending fractures after emplacement. This region may be a flooded caldera or enclosed region that has undergone structural collapse along its margins. While much of Theia Mons postdates the formation of Devana Chasma, there was evidently continued tectonic extension at the summit after the emplacement of the radar-dark materials. Where this extension has allowed the summit material to drop, the backscatter cross section (and presumably the dielectric constant) is relatively high. The change in backscatter properties occurs over vertical shifts that may be <500 m (again, we have no same-side stereo coverage for this site). Similar low radar-return behavior at elevations above ~6056 km is observed for at least two other areas along the margin of Devana Chasma (noted by arrows in Figure 6a). In all cases, topography above H_U has moderate-low radar brightness, and this effect is observed for both volcanic deposits on Theia Mons and tessera areas of Rhea.

Ozza Mons is characterized by a lower critical elevation of ~6054 km, consistent with that found at Ovda and Beta Regiones, and a similar moderate-low radar-return, low-reflectivity summit area (Figure 12). The summit area of Ozza Mons dif-

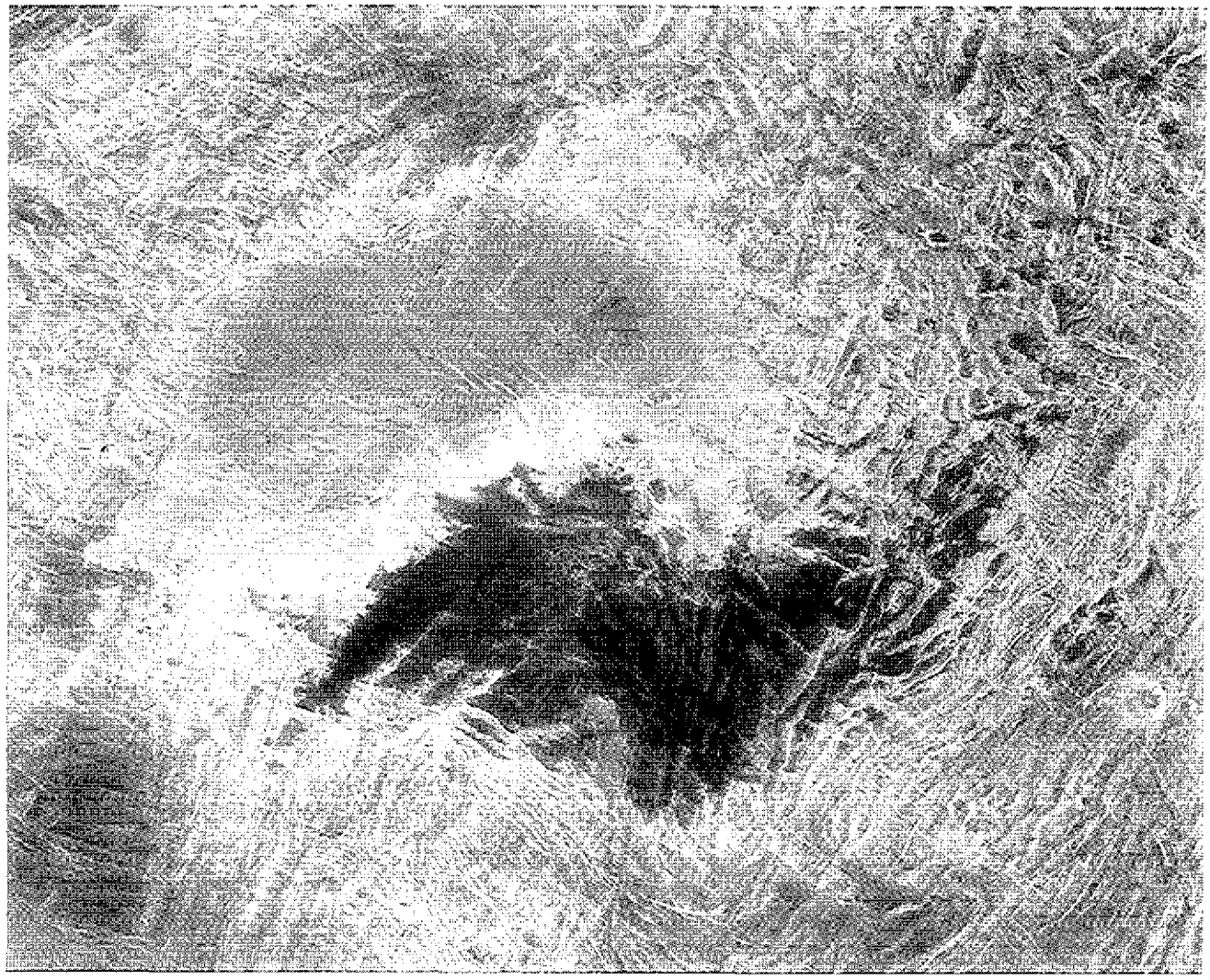

Figure 8a. Magellan radar image of festoon lava flow in Ovda regio. Image width is 263 km, centered on 6.54°S, 96.25°E. North is at the top.

fers from that of Theia Mons in having more variegated lava flows, pit craters, and small shields. Lava flows from these sources appear to have traveled down into the surrounding fractured terrain. The minimum value of H_{μ} is set by the plateau to the southeast, which is characterized by very low emissivity, high radar backscatter, and elevations just under 6057 km. There are additional areas of low radar backscatter at high elevations along Ganis Chasma, noted by arrows in Figure 7a. The transitions in surface properties with elevation are thus very similar between Ovda, Atla, and Beta Regiones.

Additional data on the nature of the radar-dark highlands are provided by the Stanford Global Vector Data Record (GVDR), which includes estimates of the near-nadir backscatter coefficient as a function of incidence angle for 16-km resolution cells across Venus [*Tyler et al.*, 1992]. We extracted echo plots for sample areas in Ovda Regio, Ozza Mons, and Theia Mons and compared these data to nearby radar-bright units and representative lowland volcanic plains. For Ovda Regio (Figure 13), the northern plains are significantly less reflective than the bright festoon flow, and the radar-dark flow is a factor of 2 (3 dB) darker still. A similar pattern is observed at Ozza Mons (Figure 14), where the summit is much darker near nadir than the plains to the west. Neither dark highland area exhibits a strong quasi-specular spike near normal incidence.

As a test, we examined the average near-nadir scattering properties of the parabolic ejecta blanket surrounding the crater Annia Faustina (Figure 15). This ejecta deposit mantles nearby lava flows, providing clear evidence for a particulate layer, and has a dielectric constant of 2-3, typical of rock fines [*Campbell*, 1994]. The near-nadir backscatter curve for the Faustina ejecta is shown in Figure 16 with the sample data for Ovda, Theia Mons, and Ozza Mons. The ejecta deposit is an excellent match for the Ozza summit data, while the Theia Mons summit and Ovda Regio flow are even less reflective.

Interpreted in terms of simple surface scattering, the highland summit regions suggest a low-reflectivity, high rms-slope surface, and the MIT Hagfors model fits to the Ovda dark flow yield mean values of ρ_o=0.07, θ_{rms}=6.4°, for the sample region used in the near-nadir study. For comparison, the Hagfors model backscatter curves for surfaces with ρ_o=0.10 and rms slopes of 1°, 2°, and 4° are shown in Figure 16. The radar-dark summit areas do have angular scattering functions consistent with relatively high rms slopes, but such a surface description is inconsistent with the low backscatter coefficients measured by the Magellan SAR sensor (cf. *Campbell and Rogers*, 1994;

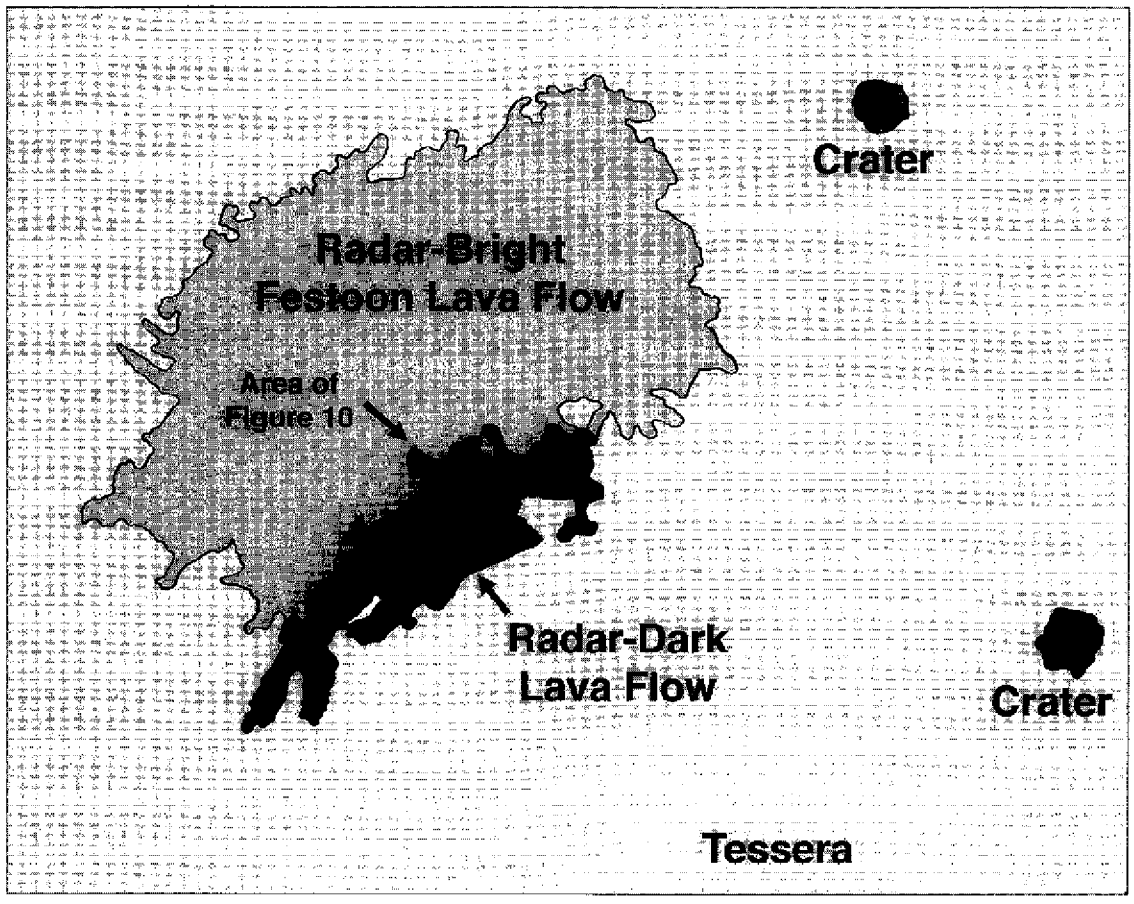

Figure 8b. Sketch map of geologic units for area shown in Figure 8a.

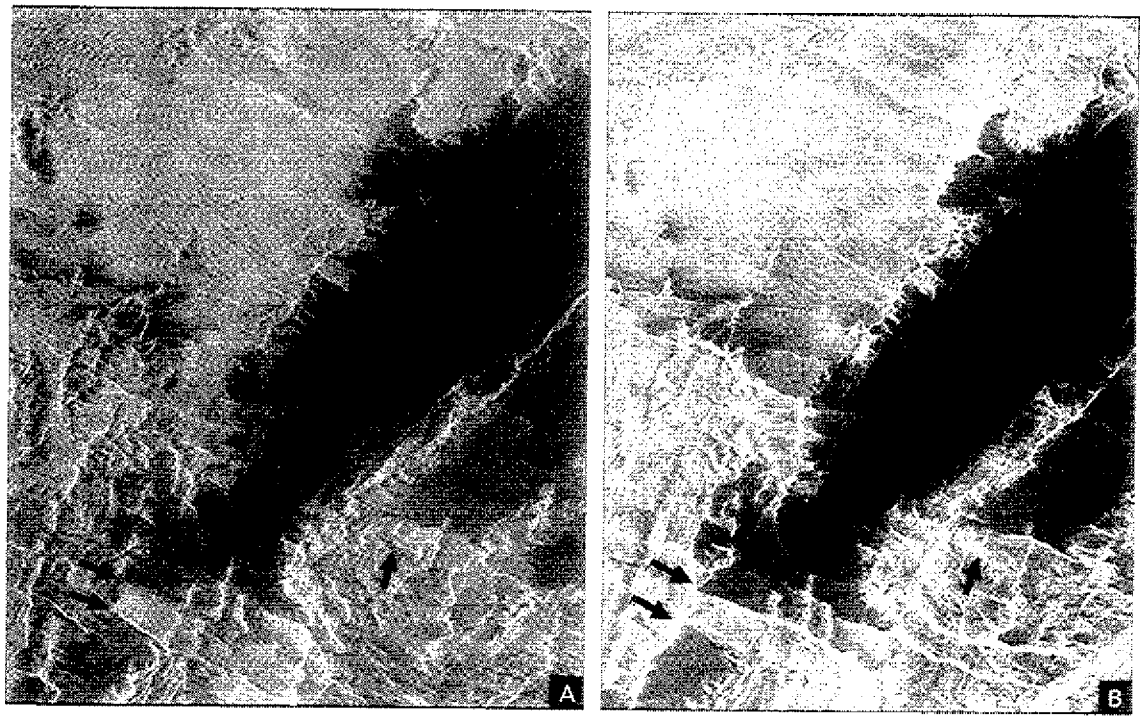

Figure 9. Magellan radar images of lava flow in central Ovda Regio. Image width is 70 km; north is at the top. Arrows denote places where the backscatter coefficient of the thick, radar-dark lava flow, which traveled from the northeast portion of the image to the southwest, changes at a shift in elevation. In one case this occurs at a graben (double arrows), and in another case it occurs as the flow descends to lower altitude with distance from the vent (single arrow). (a) Right-looking viewing geometry. (b) Left-looking viewing geometry for the same region.

Figure 10. View of contact between radar-bright and radar-dark flow materials in central Ovda Regio. Image width is 53 km; north is at the top. Note the change in surface texture between these two areas.

Figure 15). A porous deposit for which radar volume scattering and absorption are the dominant processes better fits the observations. Similar radar properties were noted for the calderas of Tepev Mons by *Campbell and Rogers* [1994], who postulated a localized ash deposit to explain their low Venera and Magellan backscatter values.

Taken together, the observations of low normal-incidence backscatter, a wide scattering function near the nadir, low backscatter at higher SAR angles (25-45°), and the muted nature of surface features in some regions are consistent with a porous surficial deposit. Since there are no indications of radar-dark wind streaks from the summit areas into neighboring high-reflectivity regions, we can infer that either the material is too coarse to be transported by the wind or that the rate of lateral transport is much less than the timescale over which high-dielectric layers or phases form. The formation of an unconsolidated layer in the highlands was suggested by *Fegley et al.* [1992] in their discussion of perovskite as a possible high-dielectric component. They point out that perovskite is converted to flourite and rutile at very high elevations on Venus and that a significant decrease in volume occurs during this transition, leading to an increase in the porosity of surface rocks. Such chemical reactions might be invoked to explain the Magellan observations, but further surface measurements are required to provide realistic constraints on the mineralogy.

5. Anomalous Behaviors at Maat Mons and Maxwell Montes

The altitude dependence of microwave properties discussed in section 4 is not observed on Maat Mons nor in several areas of Maxwell Montes. Maat Mons rises through 6054 km on its lower flanks and peaks at over 6060 km radius. Over this range, the emissivity and reflectivity show little correlation with changes in altitude. One area of moderately low emissivity occurs on the southwest flank of the mountain, and the northern flanks are influenced by the presence of fine-grained mantling material identified from both SAR images and emissivity data [*Klose et al.*, 1992; *Campbell*, 1994]. As noted above, several authors have suggested a relatively young surface age based on these radar properties. The postulated fine-grained pyroclastic deposits might impede the formation of a high-reflectivity phase or coating, but the spatial variations in E_h and ρ_o do not support this as the sole cause of lower dielectric constants on Maat Mons.

The problem is even more complicated at Maxwell Montes, where there are areas of lower radar return at elevations where, elsewhere, we observe highly reflective terrain [e.g., *Kaula et al.*, 1992]. Magellan images of two such areas are shown in Figures 17a and 17b. A profile that includes the radar-dark region in northwestern Maxwell (Figure 18) shows that elevations across this area range from 6056 to 6061 km, but the entire region is characterized by low ρ_O, high E_h, and moderate σ^o consistent with lowlands terrain. Some of the Magellan altimeter data across this portion of Maxwell were biased by the mixing of highly reflective and less reflective surfaces in a mountainous setting, but the long-wavelength to-

Figure 11. Magellan radar image of the summit of Theia Mons. The dark region is approximately 20 x 60 km in extent. Note the bright radar returns from steep scarps that ring the dark volcanic material and the lack of lava flows crossing these vertical steps. North is at the top.

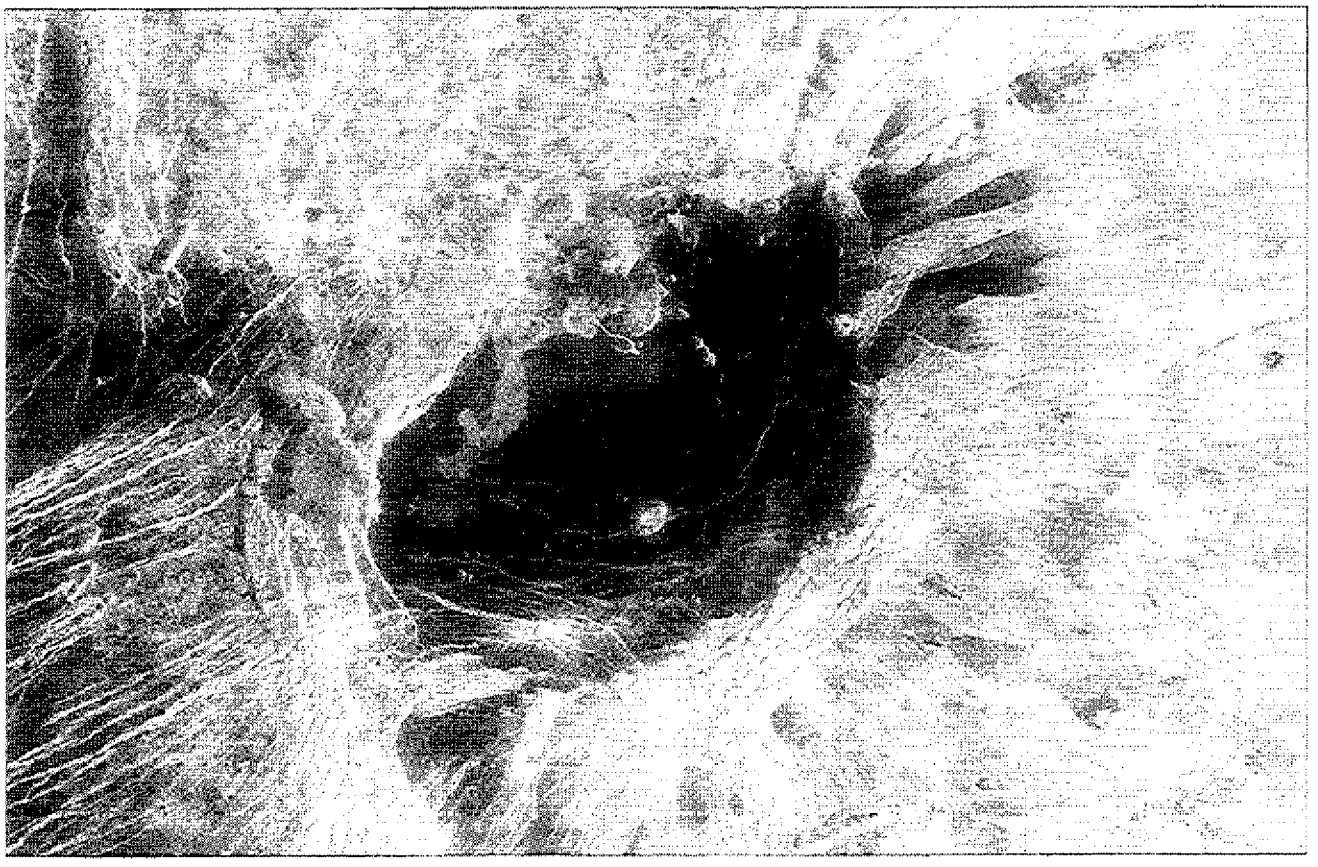

Figure 12. Magellan radar image of Ozza Mons summit. Image width is 200 km; north is at the top. Note the variegated pattern of lava flows in the summit area.

pography would have to be in error by several kilometers to place the dark material entirely below 6056 km.

What could cause the differences in surface properties between Maxwell Montes, Maat Mons, and the equatorial highlands? For Maat Mons, volcanic overprinting provides a plausible explanation if we assume that high-reflectivity material formation occurs at a constant rate through time or stopped prior to the most recent eruptions. We may explore several other potential causes for the Maxwell observations: (1) compositional differences between the radar-bright and radar-dark areas, as suggested by *Basilevsky and Head* [1995]; (2) mass wasting from steep slopes to expose fresh, unmodified surfaces in the radar-dark terrain; (3) relict reflectivity boundaries that record the surface state prior to vertical tectonic shifts (such as

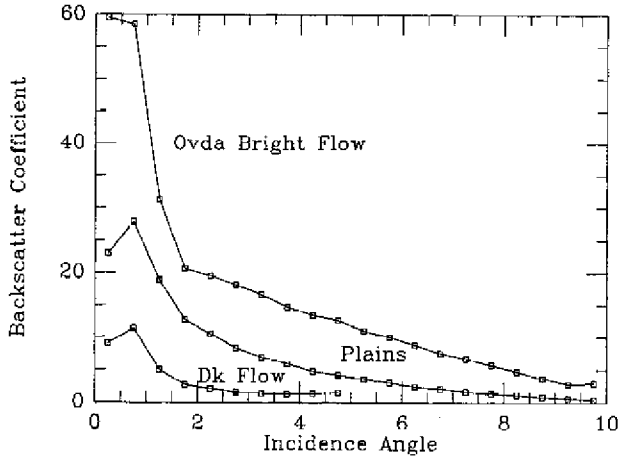

Figure 13. Near-nadir backscatter coefficient versus incidence angle for the radar-bright festoon flow, radar-dark flow, and plains north of Ovda Regio (plains sample region 6.5-7.5°N, 87.0-88.0°E).

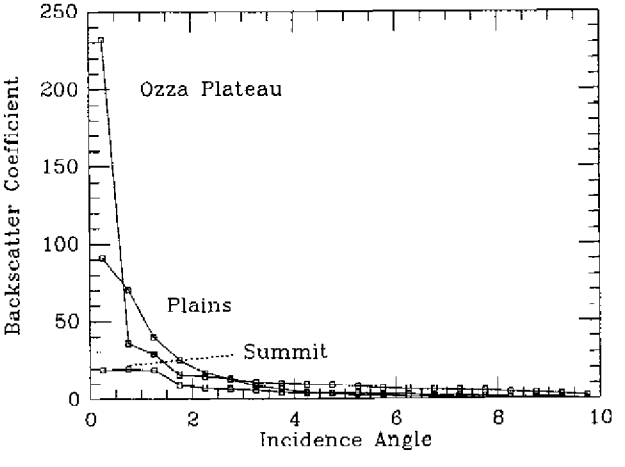

Figure 14. Near-nadir backscatter coefficient versus incidence angle for the summit of Ozza Mons, the plateau to the south of the summit, and a nearby plains region (5.2-7.0°N, 190.2-192.1°E).

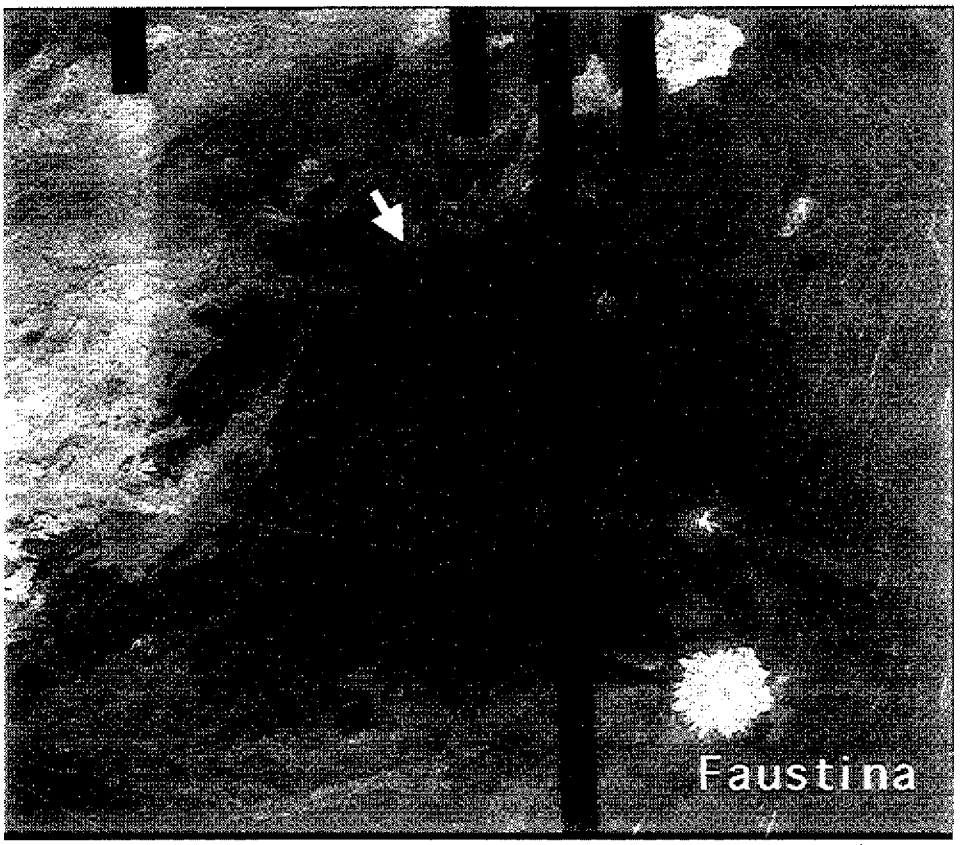

Figure 15. Magellan radar image of the ejecta deposit from crater Annia Faustina. Note that the radar-dark material mantles the rugged lava flow from Gula Mons in the region shown by the white arrow. Image width is 430 km; north is at the top.

those modeled by *Keep and Hansen* [1994]); (4) local temperature differences related to the large-scale regional topography; and (5) errors in the Magellan topography data for some regions.

Compositional differences, if they are the cause of the observed changes in surface properties, are not distinguishable (e.g., by changes in local roughness or evident remnant flow

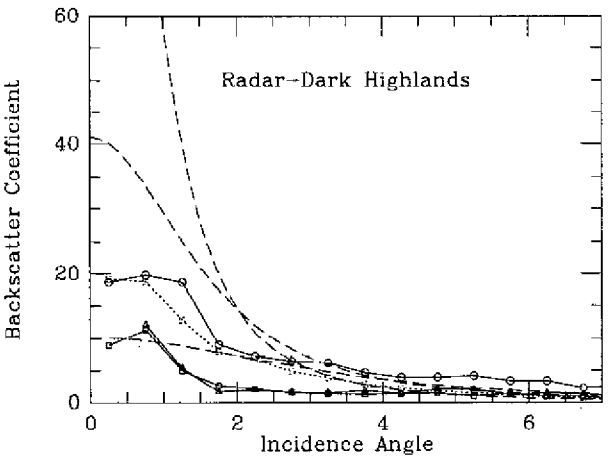

Figure 16. Near-nadir backscatter coefficient versus incidence angle for Faustina ejecta (dotted curve), Ozza Mons summit (circles), Theia Mons summit (triangles), and Ovda Regio dark flow (squares). Dashed curves represent Hagfors model scattering curves for 1°, 2°, and 4° rms slope.

lobes) in radar images of the transition zones between radar-dark and radar-bright terrain. A dark patch in southwestern Maxwell (Figure 17b) has little discernible topographic contrast (from stereo images) with the high-backscatter surroundings, but a sharply defined outer margin. It seems unlikely that this and other small isolated radar-dark patches are composed of a rock type distinct from the materials around them. We find no other evidence for preserved ancient flow boundaries or other geologic contacts between the radar-bright and radar-dark areas.

Mass wasting is a common feature throughout Maxwell Montes, though it was not widely observed elsewhere on Venus by *Malin* [1992]. There is abundant evidence for downslope movement of material, as shown by the fine patterns of linear bright streaks along the west wall of the graben in Figure 19. It is not clear whether these streaks represent high-reflectivity material moved downhill or areas from which a surficial coating of such material has been removed; both situations may occur. There are only a few obvious debris fans along the valley floors (an example is noted on Figure 19), which suggests that the mass-movement material, and thus the high-reflectivity component, is fine grained and confined to a thin surficial layer. Given that stereo images of the radar-dark regions show that they have ridges of similar slope to those in brighter areas, mass wasting alone probably cannot account for the difference between these terrains.

The ejecta blanket of Cleopatra crater, to the extent that it can be distinguished against the rugged background, covers a N-S oval within the eastern half of the mountain belt. There

Figure 17a. Magellan radar image showing the transition to lower radar return and higher emissivity west of Cleopatra crater. The southern part of this area is above the nominal critical altitude but has no associated emissivity low. The arrows denote a single laid-over ridge line for reference. Image width is 85 km.

are numerous areas north of Cleopatra with smooth image texture at the kilometer scale, which may be ponded impact melt or fine ballistic ejecta (Figure 20), and these deposits have slightly lower backscatter than the surrounding very bright terrain. In general, however, the Cleopatra ejecta deposits have radar properties similar to nearby parts of the mountains with similar elevation. Since the melt/ejecta ponds have not been deformed tectonically, we may conclude that (1) the crater is young relative to the timescale of deformation in Maxwell and (2) the crater is old relative to the timescale of high-reflectivity material formation. Combining these two observations implies that high-reflectivity material formation occurs over a shorter timescale than tectonic deformation. The dark regions elsewhere in Maxwell are thus unlikely to be relict boundaries that predate the uplift of the mountains, unless the formation rate of high-dielectric terrain has been highly variable through the recent geologic history of Venus.

The last two scenarios involving local temperature/atmospheric composition differences or elevation errors are beyond the scope of the current data to address. Local climatic differences, however, seem unlikely to occur over small isolated patches of the surface such as we see in southern Maxwell.

6. Conclusions

The analysis presented here raises significant questions for future studies of Venus surface-atmosphere interaction. Any model for highland weathering must address (1) the presence of the highly reflective material as a surface component, (2) the shift in lower critical elevation from the equator to Ishtar Terra, (3) the rapid change in surface properties with altitude at the upper critical elevation, (4) the porous erosional or depositional deposits above H_U, (5) the absence of highly reflective material at Maat Mons, and (6) the anomalous low-return areas within Maxwell Montes.

A crucial element of such a model is possible variations in surface-atmosphere reaction rates. It is possible that the process of highly reflective material formation has been active throughout the recent geologic history of Venus but that the rate has varied either spatially or temporally. Such changes might be linked to the production of specific reactive species by volcanic eruptions or large cratering events. At present, our knowledge of the lower atmosphere chemistry and surface mineralogy offers little constraint on the possible mechanisms or time variability of chemical processes in the Venus highlands. Future missions focused on measurements of the high-dielectric material composition and the abundance of reactive species near the surface are required to address these outstanding problems.

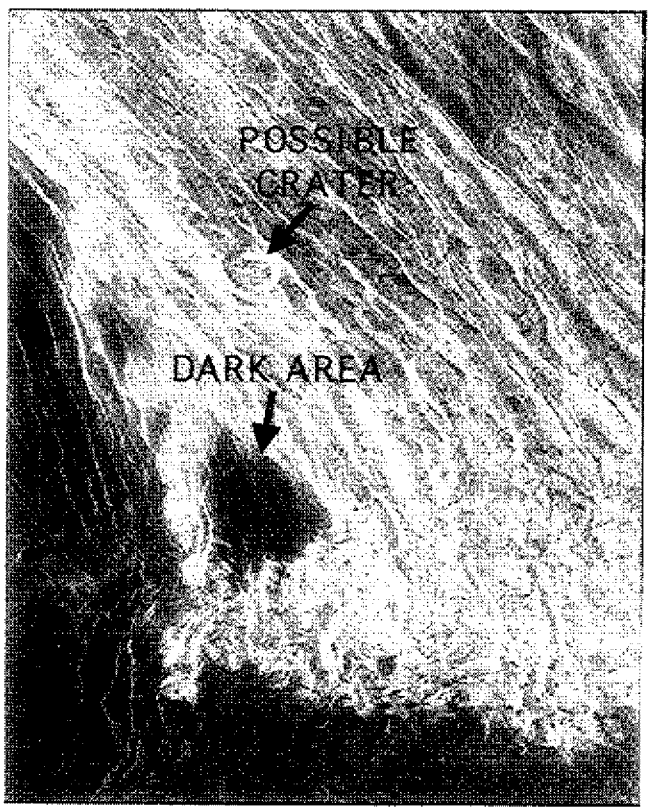

Figure 17b. Cycle 3 Magellan radar image of low-radar-return area in southern Maxwell. Note the possible impact crater just to the north. Image width is 130 km.

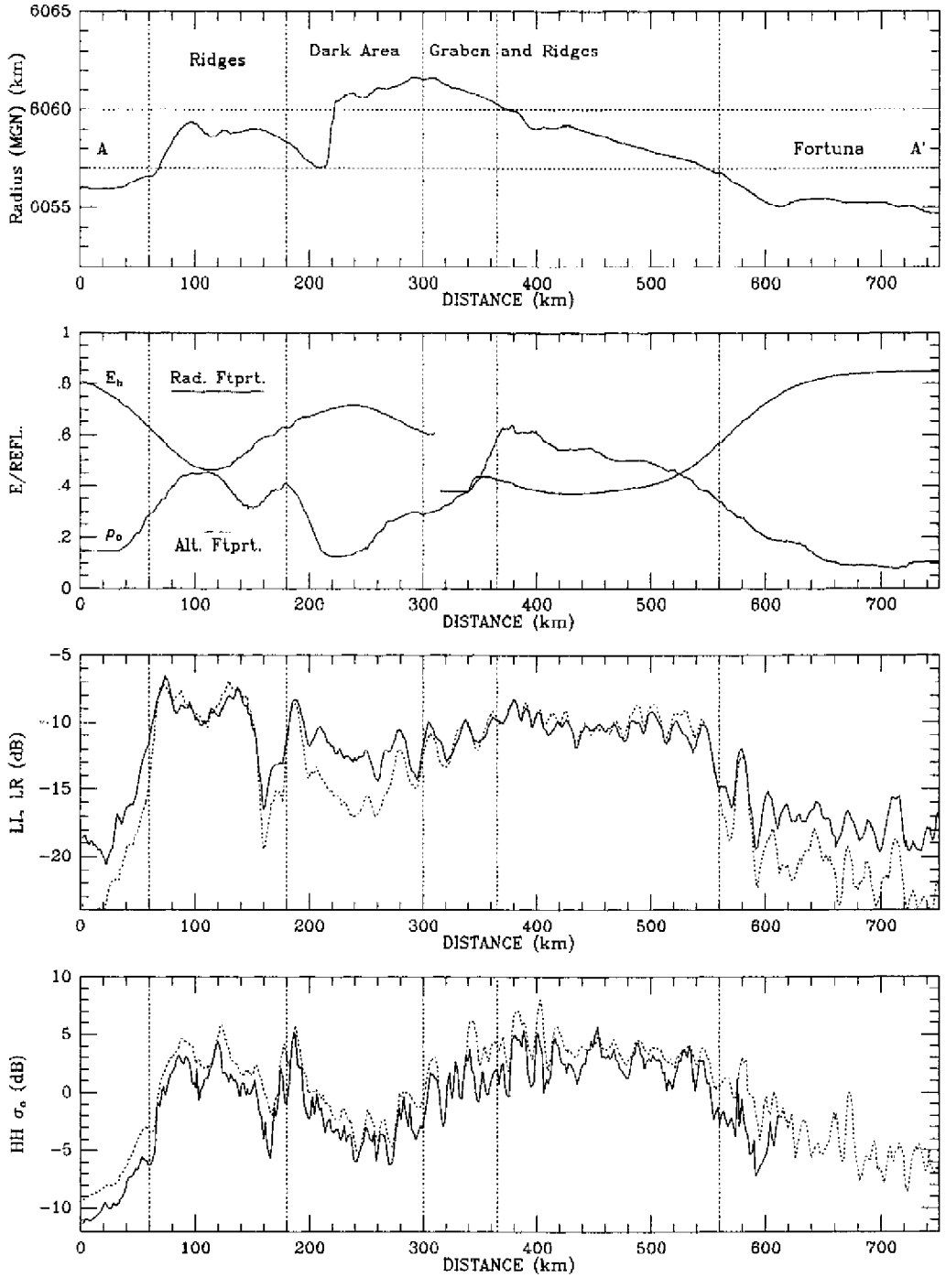

Figure 18. Profile that crosses northern Maxwell and the low-return areas (A-A' in Figure 5a). Data are plotted for planetary radius, emissivity, Fresnel reflectivity, LL (dotted) and LR (solid) backscatter cross section, and HH backscatter cross section (cycle 1 and cycle 3 data).

Appendix 1: Arecibo Data Calibration

Corrections were applied to the 1988 Arecibo data to compensate for the antenna beam pattern and effective surface-scattering area. To further refine the backscatter cross-section estimates, we used Magellan and Pioneer-Venus Orbiter (PVO) topographic maps to calculate the degree of atmospheric attenuation for any given area viewed from Earth. The atmospheric corrections were greatest (~3 dB) in the northern and southern lowlands. After these corrections, the Arecibo data were in values proportional to the backscatter coefficient (cross section per unit area), but no absolute reference level could be established from the observations. In order to provide this calibration, we utilized the regions for which Magellan and Arecibo images overlap within a 2.5° range in incidence angle. These overlap areas lie along narrow arcs in both hemispheres concentric to the radar sub-Earth point (about 0°N, 328°E for these observations).

The Magellan data are collected in HH polarization and are calibrated, while Arecibo provides LL and LR echo values

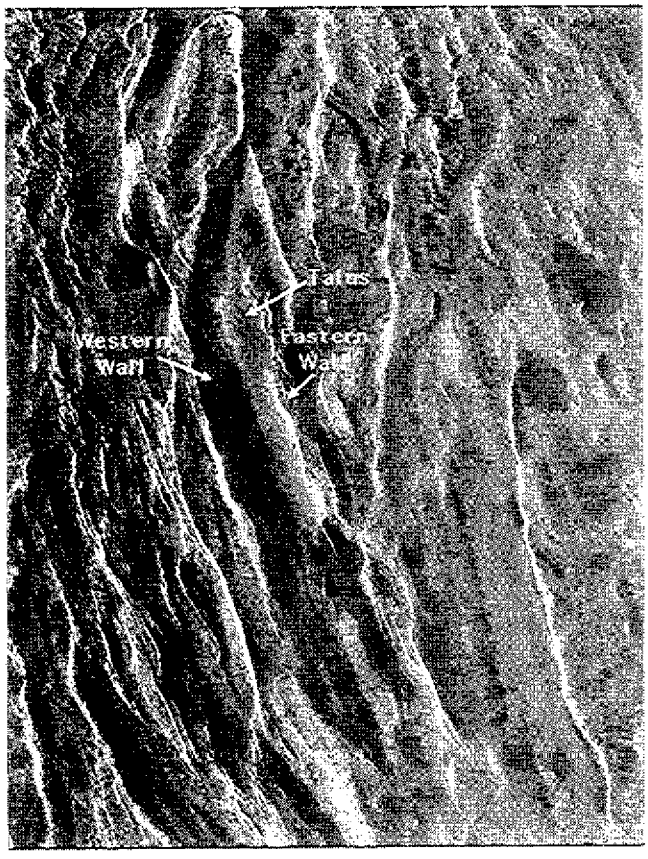

Figure 19. Magellan radar image of Maxwell Montes, showing a graben west of Cleopatra crater. Note the bright, linear streaks along the imaged western slopes of the graben, which indicate movement of material onto the valley floor. At least one possible talus deposit or debris fan is visible on the valley floor. Image width is 107 km; north is at the top.

with good relative but no absolute calibration. Aircraft radar data of terrestrial surfaces provide a means for "bootstrapping" the relationship between these two sets of measurements. Analysis of unvegetated, soil-free lava flows in Hawaii showed that the 6-cm and 24-cm radar returns at angles of 30°-60° could be well approximated by a model that combines "quasi-specular" echoes from small rock faces and "diffuse" echoes from randomly oriented cracks or edges [*Campbell et al.* 1993]. The polarization properties of these mechanisms allow the following relationships to be defined

$$\sigma^{HH} = 3\sigma^{HV} + \sigma^{Q} \tag{1}$$

$$\sigma^{LL} = 2\sigma^{HV} \tag{2}$$

$$\sigma^{LR} = 2\sigma^{HV} + \sigma^{Q} \tag{3}$$

where σ^{HV} is the power scattered by the diffuse mechanism into the linear depolarized mode, and σ^{Q} is the power scattered by small quasi-specular facets. Rearranging these equations leads to

$$\sigma^{LL} = \frac{\sigma^{HH}}{\left(0.5 + \frac{\sigma^{LR}}{\sigma^{LL}}\right)} \tag{4}$$

This equation relates the depolarized circular echo power to the HH backscatter coefficient and the circular polarization ratio, both of which are known for each pixel within the overlap region. A test of this predictive equation was made on the Hawaii data and appeared to work quite well at both 6- and 24-cm wavelengths. We carried out a best fit linear regression on the predicted and observed values of LL power to derive multiplicative correction factors for the Arecibo data. While we cannot verify the absolute calibration of the Magellan images, this technique at least makes it possible to compare the Magellan and Arecibo data sets.

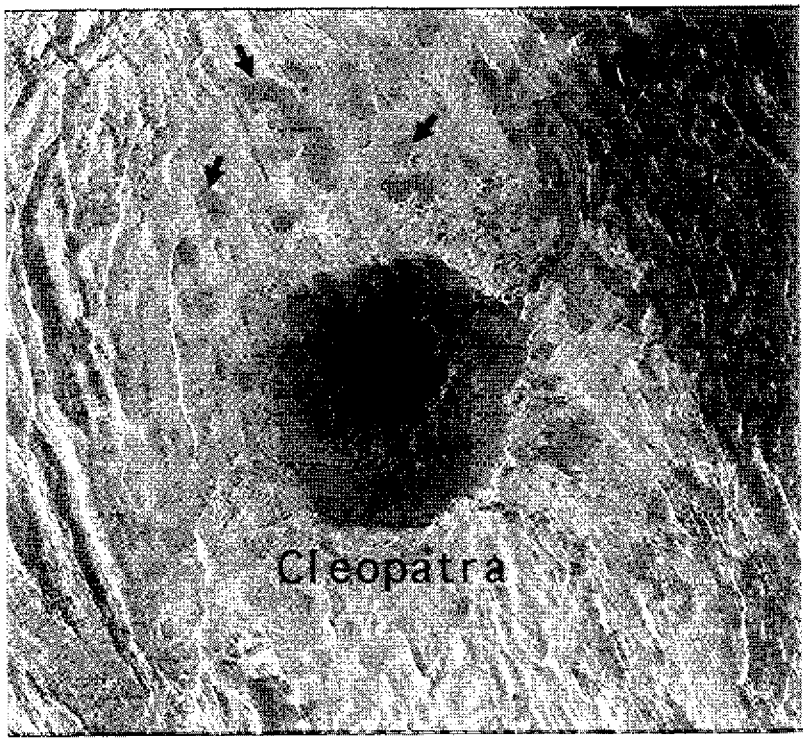

Figure 20. Magellan radar image of Cleopatra crater and associated areas of smooth ponded material (noted by arrows). Image width is 280 km; north is at the top.

Appendix 2: Magellan Topographic Data

In the course of our study of the Venus highlands, we found that some areas have anomalous elevation changes, relative to their surroundings, in the global topographic map (the GTDR [*Ford and Pettengill*, 1992]). This digital elevation model was produced by Gaussian filtering of the individual altimeter footprints to a 5.4-km map base. In the areas with anomalous relief, the echo traces were often characterized by multiple peaks or high background signal levels, making the derived radius value suspect. In an effort to quantify the reliability of each altimeter measurement, we examined the 302 range bins, $R(k)$, that make up each echo trace. The multiple radar looks which form the profile were migrated during processing to produce a range-sharpened echo, and a Hagfors-function template was fit to the data to estimate the planetary radius [*Ford and Pettengill*, 1992]. The template area is 50 bins wide, and the echoes within this region are expected to represent the near-nadir return from the surface. Our primary concern is the degree to which this particular portion of the echo trace is unique (that is, could other portions of the profile also be potential subspacecraft returns?). In areas where the terrain is highly variable in its large-scale roughness or where off-nadir surfaces have very high reflectivity, it is possible that the echo profile could be ambiguous.

A quality factor Q was defined as the mean normalized cross correlation between the 50-bin-wide best fit template function $T(k)$ and the remainder of the echo trace:

$$Q = \frac{\sum_{k=1}^{50} T(k)\,R(k+\delta)}{\sum_{k=1}^{50} T(k)^2} \qquad (5)$$

where δ is the lag in range bins between the range-sharpened profile $R(k)$ and the best fit template function. The lag was varied so that the template never overlapped with itself, since the autocorrelation of this region formed the normalization term. Higher values of Q thus correspond to less unique solutions for the surface radius, reflectivity, and rms slope, since the chosen location for the template may be ambiguous with other portions of the profile. For the profiles presented here, we discarded footprints for which Q>0.60 (an empirical cutoff that appeared to remove only very noisy footprints) and resampled the remaining data with a 16-km-radius Gaussian weighting function.

Acknowledgments. The authors thank Alice Hine for much assistance in mapping the Arecibo Venus data. Thanks also to Richard Simpson, Mike Shepard, Nick Stacy, and Mark Bulmer for numerous helpful discussions, and to Peter Ford for aid in setting up the atmospheric corrections. D. Senske and an anonymous reviewer provided constructive reviews. This work was supported in part by a grant from the NASA Planetary Geology and Geophysics Program (NAG5-4545).

References

Arvidson, R. E., R. Greeley, M. C. Malin, R. S. Saunders, N. Izenberg, J. J. Plaut, E.R. Stofan, and M. K. Shepard, Surface modification of Venus as inferred from Magellan observations of plains, *J. Geophys. Res.*, *97*, 13303-13318, 1992.

Arvidson, R. E., R. A. Brackett, M. K. Shepard, N. R. Izenberg, B. Fegley, and J. J. Plaut, Microwave signatures and surface properties of Ovda Regio and surroundings, Venus, *Icarus*, *112*, 171-186, 1994.

Barsukov, V. L., et. al., The geology and geomorphology of the Venus surface as revealed by the radar images obtained by Veneras 15 and 16, *J. Geophys. Res.*, *91*, 378-398, 1986.

Basilevsky, A. T., and J. W. Head, The age of deformations and composition inhomogeneities in Maxwell Montes on Venus, *Sol. Syst. Res.*, *29*, 335-345, 1995.

Brackett, R. A., B. Fegley, and R. E. Arvidson, Volatile transport on Venus and implications for surface geochemistry and geology, *J Geophys. Res.*, *100*, 1553-1564, 1995.

Campbell, B. A., Merging Magellan emissivity and SAR data for analysis of Venus dielectric properties, *Icarus*, *112*, 187-203, 1994.

Campbell, B. A., and D. B. Campbell, Analysis of volcanic surface morphology on Venus from comparison of Arecibo, Magellan, and terrestrial airborne radar data, *J. Geophys. Res.*, *97*, 16,293-16,314, 1992.

Campbell, B. A., and P. G. Rogers, Bell Regio, Venus: Integration of remote sensing data and terrestrial analogs for geologic analysis, *J Geophys. Res.*, *99*, 21153-21171, 1994.

Campbell, B. A., and M. K. Shepard, Lava flow surface roughness and depolarized radar scattering, *J. Geophys. Res.*, *101*, 18,941-18,952, 1996.

Campbell, B. A., R. E. Arvidson, and M.K. Shepard, Radar polarization properties of volcanic and playa surfaces: Applications to terrestrial remote sensing and Venus data intepretation, *J. Geophys. Res.*, *98*, 17,099-17,114, 1993.

Campbell, D. B., J. W. Head, J. K. Harmon, and A. A. Hine, Venus: Identification of banded terrain in the mountains of Ishtar Terra, *Science*, *221*, 644-647, 1983.

Campbell, D. B., J. W. Head, J. K. Harmon, and A. A. Hine, Venus: Volcanism and rift formation in Beta Regio, *Science*, *226*, 167-170, 1984.

Fegley, B., A. H. Trieman, and V. L. Sharpton, Venus surface mineralogy: Observational and theoretical constraints, *Proc. Lunar Planet. Sci. Conf. 22nd*, 3-19, 1992.

Fegley, B., G. Klingelhofer, K. Lodders, and T. Widemann, Geochemistry of surface-atmosphere interactions on Venus, in *Venus II*, pp. 591-636, Univ. of Ariz. Press, Tucson, 1997.

Ford, P. G., and G. H. Pettengill, Venus topography and kilometer-scale slopes, *J. Geophys. Res.*, *97*, 13,102-13,114, 1992.

Hagfors, T., Backscattering from an undulating surface with applications to radar returns from the Moon, *J. Geophys. Res.*, *69*, 3779-3784, 1964.

Hagfors, T., and D. B. Campbell, Radar backscattering from Venus at oblique incidence at a wavelength of 70 cm, *Astron. J.*, *79*, 493-501, 1974.

Haldemann, A. F. C., D. O. Muhleman, B. J. Butler, and M. A. Slade, The western hemisphere of Venus: 3.5 cm dual circular-polarization radar images, *Icarus*, *128*, 398-414, 1997.

Hapke, B., Coherent backscatter and the radar characteristics of outer planets satellites, *Icarus*, *88*, 407-417, 1990.

Head, J. W., L. S. Crumpler, J. C. Aubele, J. E. Guest, and R. S. Saunders, Venus volcanism: Classification of volcanic features and structures, associations, and global distributions from Magellan data, *J. Geophys. Res.*, *97*, 13,153-13,198, 1992.

Jurgens, R. F., M. A. Slade, and R. S. Saunders, Evidence for highly reflecting materials on the surface and subsurface of Venus, *Science*, *240*, 1021-1023, 1988.

Kaula, W.M., D.L. Bindschadler, D.L., R.E. Grimm, V.L. Hansen, K.M. Roberts, and S.E. Smrekar, Styles of deformation in Ishtar Terra and their implications, *J. Geophys. Res.*, *97*, 16085-16120, 1992.

Keep, M., and V. L. Hansen, Structural history of Maxwell Montes, Venus: Implications for Venus mountain belt formation, *J. Geophys. Res.*, 99, 26,015-26,028, 1994.

Klose, K. B., J. A. Wood, and A. Hashimoto, Mineral equilibria and the high radar reflectivity of Venus mountaintops, *J. Geophys. Res.*, *97*, 16,353-16370, 1992.

Malin, M., Mass movements on Venus: Preliminary results from Magellan Cycle 1 observations, *J. Geophys. Res.*, *97*, 16,337-16,352, 1992.

McGill, G.E., J.L. Warner, M.C. Malin, R.E. Arvidson, E. Eliason, S. Nozette, and R.D. Reasenberg, Topography, surface properties, and tectonic evolution, in *Venus*, pp. 69-130, Univ. of Ariz. Press, Tucson, 1983.

Moore, H. J., J. J. Plaut, P. M. Schenck, and J. W. Head, An unusual volcano on Venus, *J. Geophys. Res.*, *97*, 13,479-13,494, 1992.

Ostro, S. J., et al., Europa, Ganymede, and Callisto: New radar results from Arecibo and Goldstone, *J. Geophys. Res.*, *97*, 13,091-13,102, 1992.

Pettengill, G. H., P. G. Ford, and B. D. Chapman, Venus: Surface electromagnetic properties, *J. Geophys. Res.*, *93*, 14,881-14,892, 1988.

Pettengill, G. H., P. G. Ford, and R. J. Wilt, Venus surface radiothermal emission as observed by Magellan, *J. Geophys. Res.*, *97*, 13,091-13,102, 1992.

Pettengill, G. H., Tellurium on Venus: A highlands thermometer?, *EOS Trans. AGU*, *77(46)*, Fall Meet. Suppl., F440, 1996.

Pettengill, G. H., P. G. Ford, and R. A. Simpson, Electrical properties of the Venus surface from bistatic radar observations, *Science*, *272*, 1628-1631, 1996.

Rignot, E., Backscatter model for the unusual radar properties of the Greenland Ice Sheet, *J. Geophys. Res.*, *100*, 9389-9400, 1995.

Robinson, C. R., Large-scale volcanic activity at Maat Mons: Can this explain fluctuations in atmospheric chemistry observed by Pioneer-Venus?, *J. Geophys. Res.*, *100*, 11755-11764, 1995.

Robinson, C. R., and J. A. Wood, Recent volcanic activity on Venus: Evidence from radiothermal emissivity measurements, *Icarus*, *102*, 26-39, 1993.

Saunders, R. S., et al., Magellan mission summary, *J. Geophys. Res.*, *97*, 13,067-13,090, 1992.

Senske, D.A., D.B. Campbell, E.R. Stofan, P.C Fisher, J.W. Head, N. Stacy, J.C. Aubele, A.A. Hine, and J.K. Harmon, Geology and tectonics of Beta Regio, Guinevere Planitia, Sedna Planitia, and Western Eistla Regio, Venus: Results from Arecibo data, *Earth Moon Planets*, *55*, 163-214, 1991.

Senske, D. A., G. G. Schaber, and E. R. Stofan, Regional topographic rises on Venus: Geology of Western Eistla Regio and comparison to Beta Regio and Atla Regio, *J. Geophys. Res.*, *97*, 13,395-13,420, 1992.

Shepard, M. K., R. E. Arvidson, R. A. Brackett, and B. Fegley, A ferroelectric model for the low emissivity highlands on Venus, *Geophys. Res. Lett.*, *21*, 469-472, 1994.

Solomon, S. C., et. al., Venus tectonics: An overview of Magellan observations, *J. Geophys. Res.*, *97*, 13,199-13,255, 1992.

Stofan, E. R., J. W. Head, D. B. Campbell, S. H. Zisk, A. F. Bogomolov, O. N. Rzhiga, A. T. Basilevsky, and N. Armand, Geology of a rift zone on Venus: Beta Regio and Devana Chasma, *Geol. Soc. Am. Bull.*, *101*, 143-156, 1989.

Tryka, K. A. and D. O. Muhleman, Reflection and emission properties on Venus: Alpha Regio, *J. Geophys. Res.*, *97*, 13,379-13,394, 1992.

Tyler, G.L., R.A. Simpson, M.J. Maurer, and E. Holmann, Scattering properties of the venusian surface: Preliminary results from Magellan, *J. Geophys. Res.*, *97*, 13,115-131,140, 1992.

Wilt, R.J., A study of areas of low radiothermal emissivity on Venus, Ph.D. dissertation, Massachusetts Inst. of Technol., Cambridge, 175 pp., 1992.

Wood, J.A., Rock weathering on the surface of Venus, in *Venus II*, pp. 637-666, Univ. of AZ Press, Tucson, 1997.

B. A. Campbell, Center for Earth and Planetary Studies, Smithsonian Institution, MRC 315, Washington, DC 20560-0315. (campbell@ceps.nasm.edu)

D. B. Campbell, National Astronomy and Ionosphere Center, Cornell University, Space Sciences Building, Ithaca, NY 14853.

C. H. DeVries, Department of Physics and Astronomy, University of Massachusetts, Amherst, MA 01003.

(Received July 23, 1997; revised October 6, 1998;
accepted October 7, 1998)